



**HAL**  
open science

# Hybrid centrifugal spreading model to study the fertiliser spatial distribution and its assessment using the transverse coefficient of variation

Sylvain Villette, Emmanuel Piron, Denis Miclet

► **To cite this version:**

Sylvain Villette, Emmanuel Piron, Denis Miclet. Hybrid centrifugal spreading model to study the fertiliser spatial distribution and its assessment using the transverse coefficient of variation. *Computers and Electronics in Agriculture*, 2017, 137, pp.115-129. 10.1016/j.compag.2017.03.023 . hal-01601353

**HAL Id: hal-01601353**

**<https://hal.science/hal-01601353>**

Submitted on 4 Feb 2019

**HAL** is a multi-disciplinary open access archive for the deposit and dissemination of scientific research documents, whether they are published or not. The documents may come from teaching and research institutions in France or abroad, or from public or private research centers.

L'archive ouverte pluridisciplinaire **HAL**, est destinée au dépôt et à la diffusion de documents scientifiques de niveau recherche, publiés ou non, émanant des établissements d'enseignement et de recherche français ou étrangers, des laboratoires publics ou privés.



Distributed under a Creative Commons Attribution - ShareAlike 4.0 International License

1  
2  
3  
4  
5  
6  
7  
8  
9  
10  
11  
12  
13  
14  
15  
16  
17  
18  
19  
20  
21

**Preprint of :**

Villette, S., Piron, E., & Miclet, D. (2017). Hybrid centrifugal spreading model to study the fertiliser spatial distribution and its assessment using the transverse coefficient of variation. *Computers and Electronics in Agriculture*, 137, 115-129.  
<http://doi.org/10.1016/j.compag.2017.03.023>

<http://www.sciencedirect.com/science/article/pii/S0168169917304325>

1                    **Hybrid centrifugal spreading model to study the fertiliser spatial**  
2                    **distribution and its assessment using the transverse coefficient of variation**  
3  
4

5                    S Villette <sup>a,b\*</sup>, E Piron <sup>c</sup>, D Miclet <sup>c</sup>  
6

7 <sup>a</sup> Agroécologie, AgroSup Dijon, INRA, Univ. Bourgogne Franche-Comté, F-21000 Dijon,  
8 France

9 <sup>b</sup> Equipe Agroéquipements, AgroSup Dijon, BP 87999, 21079 Dijon Cedex, France

10 <sup>c</sup> IRSTEA, Les Palaquins, 03150 Montoldre, France  
11

12 \* Corresponding author.

13 E-mail address: sylvain.villette@agrosupdijon.fr  
14

15 **Abstract**  
16

17 Studying centrifugal spreading by carrying out field or in-door experiments using fertiliser  
18 collection trays is tedious and labour intensive. This is particularly true when several  
19 implementation methods need to be compared, numerous replications are required or fertiliser  
20 sample characterisation is required. To circumvent cumbersome experiments, an alternative  
21 approach consists in performing in silico studies. In order to reach this objective, a hybrid  
22 centrifugal spreading model is designed by combining theoretical fertiliser motion equations  
23 with statistical information. The use of experimental measurements to characterise fertiliser  
24 properties, outlet velocity, angular mass flow distribution and spread pattern deposition,  
25 ensure a realistic calibration of the model. Based on this model, static spread patterns and  
26 transverse distributions are computed for a virtual twin-disc spreader. The number of fertiliser  
27 granules used to compute a spread pattern is deduced from the target application rate while  
28 the granule properties and their motion parameters are randomly selected from pre-established  
29 statistical distributions. This Monte Carlo process reproduces the random variability of  
30 fertiliser spread pattern depositions. Using this model, simulations demonstrate the mean and  
31 standard deviation of CV value decrease with the application rate. The CV mean value also  
32 decreases with the collection tray surface, while the standard deviation decreases with the  
33 collection tray length. Mathematical relationships are deduced from simulation results to  
34 express the mean and standard deviation of the CV as functions of the application rate and  
35 collection tray surface or length. The simulation model is also used to compare spreader test  
36 methods and study the influence of some fertiliser particles properties on the transverse  
37 distribution.  
38  
39

40 **Keywords**  
41

42 Centrifugal spreading, Coefficient of Variation, Model, Monte Carlo, Simulation, Virtual  
43 spreader  
44  
45  
46

1	<b>Notation</b>	
2		
3	$a$	regression parameter
4	$A_p$	particle frontal area, $m^2$
5	$b$	regression parameter
6	$c$	regression parameter
7	$C_d$	drag coefficient
8	CV	transverse coefficient of variation, %
9	CV <sub>geom</sub>	geometrical component of the CV, %
10	CV <sub>k</sub>	value of the CV obtained when the collection tray width is $w_k$ , %
11	$D$	continuous random variable, m
12	$d_p$	fertiliser granule diameter, m
13	$d_{pi}$	diameter of the $i^{\text{th}}$ fertiliser granule, m
14	$F_D(d_p)$	cumulative frequency function of the granule diameter
15	$f_D(d_p)$	probability density function of the granule diameter
16	$g$	acceleration due to gravity, $m\ s^{-2}$
17	$G_D(d_p)$	cumulative mass distribution function of the granule diameter
18	$G_M(\theta_{vane})$	cumulative mass flow distribution with respect to the vane location
19	$g_M(\theta_{vane})$	mass flow distribution with respect to the vane location
20	$h_{vane}$	height of the outer extremity of the vane, m
21	$K$	constant, $m^3$
22	$K_a$	aerodynamic coefficient, $m^{-1}$
23	$l_{tray}$	length of the collection tray, m
24	$L_w$	swath spacing, m
25	$m$	particle mass, kg
26	$m(d_p)$	mass of a granule of diameter $d_p$ , kg
27	$m_i$	mass of the $i^{\text{th}}$ fertiliser granule, kg
28	$m_{tot}$	total mass of fertiliser ejected by the two discs of the virtual spreader, kg
29	$n_{disc}$	number of granules ejected by one disc of the virtual spreader
30	$(O, i, j, k)$	Cartesian frame centred on the disc centre, with $j$ oriented in the travel direction
31		
32	$q_t$	target application rate, kg/ha
33	$q_f$	in-field target rate, kg/ha
34	$r$	Pearson correlation coefficient
35	$r_{vane}$	radius of the vane, m
36	$s_{disc}$	distance between the two disc axles of the virtual spreader, m
37	$t$	time, s
38	$v_H$	horizontal component of the outlet velocity, $m\ s^{-1}$
39	$v_{out}$	outlet velocity, $m\ s^{-1}$
40	$(v_x, v_y, v_z)$	velocity components of the granule during the ballistic flight, m
41	$(v_{xout}, v_{yout}, v_{zout})$	components of the outlet velocity, $m\ s^{-1}$
42	$w_k$	width of the collection trays
43	$(x, y, z)$	coordinates of the granule, m
44	$(x_{out}, y_{out}, z_{out})$	coordinates of the granule when it leaves the vane, m
45	$\alpha_{lv}$	pitch angle of the vane, $^\circ$
46	$\alpha_{set}$	setting angle of the virtual spreader, $^\circ$
47	$\Delta l_{grid}$	grid sampling interval along the travel direction, m
48	$\Delta w_{grid}$	grid sampling interval along the transverse direction, m
49	$\theta_{out}$	horizontal outlet angle of the granule when it leaves the vane, $^\circ$
50	$\theta_{raj}$	horizontal orientation of the outlet velocity with respect to $i$ , $^\circ$

1	$\theta_{vane}$	angular location of the vane with respect to $i$ , °
2	$\mu_{CV}$	mean value of the CV, %
3	$\mu_{ln}$	fitting parameter of the cumulative mass distribution
4	$\mu\theta_{out}$	mean value of the horizontal outlet angle, °
5	$\xi$	variable of integration, m
6	$\rho$	density of the fertiliser granule, kg m <sup>-3</sup>
7	$\rho_{air}$	air density, kg m <sup>-3</sup>
8	$\sigma\theta_{out}$	standard deviation of the horizontal outlet angle, °
9	$\sigma\Omega_{out}$	standard deviation of the vertical outlet angle, °
10	$\sigma_{CV}$	standard deviation of CV, %
11	$\sigma_{ln}$	fitting parameter of the cumulative mass distribution
12	$\omega$	rotational speed of the spinning disc, rad s <sup>-1</sup>
13	$\Omega_{out}$	vertical outlet angle of the granule, °
14	$\Omega_{vane}$	vertical angle of the vane, °
15		
16		
17		

## 1 1. Introduction

2  
3 In agriculture, the objective of mineral fertiliser supplies is to provide the right rate of  
4 nutrients to cultivated plants. Because of their low cost and high productivity, centrifugal  
5 spreaders are widely used for this application aiming to spread fertiliser at a target rate with  
6 an acceptable uniformity in the field. For 50 years several works have demonstrated the  
7 negative effects of non-uniform spatial distributions concerning environmental impacts  
8 ([Tissot et al., 2002](#)) and yield or economical losses ([Horrell et al., 1999](#); [Jensen and Pesek,](#)  
9 [1962](#); [Miller et al., 2009](#); [Richards and Hobson, 2013](#); [Søgaard and Kierkegaard, 1994](#); [Tissot](#)  
10 [et al., 1999](#)). For the same decades, numerous works have been devoted to the measurement  
11 of fertiliser distributions, the assessment of distribution quality and the understanding of  
12 spread patterns. Throughout the world, transverse tray tests are traditionally performed to  
13 measure the spreading uniformity according to various standards such as: [ISO Standard](#)  
14 [5690/1 \(1985\)](#); [ASAE Standards S341.2 \(1999\)](#); [EN 13739-2 \(2003\)](#); Spreadmark code of  
15 practice ([New Zealand Fertiliser Quality Council \(2015\)](#)) or ACCU Spread ([Australian](#)  
16 [Fertiliser Services Association, 2001](#)). The experimental transverse distribution is then used to  
17 compute the coefficient of variation CV after overlapping. This CV value is used to quantify  
18 the spreading quality, define the appropriate swath spacing according to the fertiliser and the  
19 spreader setting, and thus certify the spreader bout width.

20 Some studies have addressed the comparison of transverse distribution measurement methods.  
21 Several works investigated the influence of the collection systems. [Parish \(1986\)](#) compared  
22 twelve collection methods in laboratory conditions using a manually-operated rotary spreader  
23 and two granular materials. The maximal effective swath width of this spreader was 4.3 m.  
24 Each test run consisted of three passes and three replications where carried out. Using the  
25 results obtained in this previous work, [Parish and de Visser \(1989\)](#) analysed the effect of the  
26 collection tray width on the CV value. In field, [Parish et al. \(1987\)](#) compared the crop  
27 response quality assessed by a horticulturist with the fertiliser rates deduced from transverse  
28 distribution measurements. Three collection methods were compared using three replications  
29 for each test. All these studies demonstrated that, depending on the test method, major  
30 differences occurred in the measurement of the transverse distribution. Therefore, the authors  
31 highlighted the importance of using the same test method for comparisons of spreader  
32 performance. Moreover regarding the low throwing distance of the spreader chosen for these  
33 studies and the low number of replications, these works illustrate the difficulties of carrying  
34 out such experiments.

35 To perform statistical comparisons of six international spreader tests, [Jones et al. \(2008\)](#)  
36 carried out a huge experimental work by using 18 transverse rows of 80 trays each. The  
37 experiments were carried out with urea, for three application rates and two replications so that  
38 36 transverse distributions were obtained for each spreading situation. The bout width of the  
39 spreader was 15 m. Concerning the prediction of the certifiable working width, the authors  
40 concluded that the ACCU Spread test method ([Australian Fertiliser Services Association,](#)  
41 [2001](#)) was superior to the other tested standards because it uses two rows of collector trays  
42 and multiple passes. [Jones et al. \(2008\)](#) concluded multiple rows of trays, multiple passes of  
43 the spreader and long trays can improve the accuracy of transverse tests.

44 Since the transverse distribution results from the combination of numerous parameters, it only  
45 provides a limited piece of information concerning the spread pattern. Thus, transverse tests  
46 are not efficient to study how mechanical parameters or fertiliser characteristics affect the 2D  
47 spread pattern deposition. This was illustrated by [Piron and Miclet \(2005\)](#) who showed that  
48 different 2D static spread patterns can yield to similar transverse patterns. Unfortunately, the  
49 measurement of the 2D static spread pattern is very tedious when a grid of collection trays is  
50 used, because of the wide size of spreader footprints and the high number of trays required to

1 cover this area. Moreover, for indoor test, the high throwing distance of recent spreaders  
2 would require very expensive infrastructures. To circumvent these difficulties, [Piron and](#)  
3 [Miclet \(2005\)](#) developed a rotating test bench called CEMIB. With this method, the spreader  
4 is rotated during the spreading and a radial row of collection trays equipped with load cells  
5 records the cumulated mass of fertiliser according to the angular orientation of the spreader.  
6 The static spread pattern is then derived from the cumulated mass and the CV of the  
7 transverse distribution can be deduced ([EN 13739-2, 2011](#)). The measurement of the 2D  
8 spread pattern is of particular interest to improve the understanding of the spread pattern  
9 formation, the understanding of mechanical parameter effects and more generally to design  
10 new spreader. It is also useful to calibrate or validate spreading models.

11 Recently, [Cool et al. \(2015\)](#) addressed the design of a simplified measurement technique to  
12 estimate the 2D static spread pattern in field, using a limited number of collection trays placed  
13 on a square or polar grid. The results of these two sampling techniques were compared with  
14 the results obtained with a transverse test. Tests were carried out with a spreader whose  
15 setting corresponded to 15 m bout width for ammonium nitrate fertiliser. Tests were  
16 performed for three fertilisers without replication. The authors observed large differences in  
17 the CV values deduced from the three measurement techniques and highlighted the  
18 importance of using the same measurement techniques to compare spread patterns. As this  
19 kind of experiments is tedious and does not make possible a sufficient number of replications  
20 to compare significant values, this work illustrates the need of alternative approaches when  
21 the design or the assessment of new spreading quality measurement techniques is required.

22  
23 The complexity and the labour-intensive nature of experimental measurements further  
24 increase when the study is not limited to the fertiliser mass distribution but aims to analyse the  
25 size or the nutrient formulation of the granules with respect to their spatial distribution. For  
26 example, very few studies investigated the effect of fertiliser particle size on spread  
27 distribution. [Pettersen et al. \(1991\)](#) studied the spatial distribution of fertiliser particle size  
28 using a twin disc spreader. Experiments were limited to the choice of one fertiliser, one  
29 spreader setting, one feeding flow rate and one measurement of the 2D stationary spread  
30 pattern. A set of 884 collected samples was analysed by image processing technique to draw  
31 the spatial distribution of the particle size. Thirty years later, [Yule \(2011\)](#) attempted to study  
32 the effect of fertiliser particle size on spread distribution. The transverse distribution of the  
33 percentage of particle size was drawn for two loads of superphosphate having different  
34 granule size distributions. [Yule \(2011\)](#) used these experimental results to simulate the  
35 transverse distribution of other materials with other particle size characteristics. Nevertheless,  
36 the author underlined the work is limited to representing only one particular spreading  
37 situation: one spreader with one fertiliser and one setting. [Yule \(2011\)](#) concluded that further  
38 work would be required but analysing each tray from field testing was too time-consuming  
39 and no laboratory measurement techniques were adapted for this kind of study at the present  
40 time.

41 The study of the spatial distribution of fertiliser granules according to their physical properties  
42 is of particular interest in the case of blended fertilisers. As these materials are produced by  
43 mixing mechanically single products, their components differ in the physical properties (size,  
44 shape and density). These differences can involve segregation of the fertiliser components  
45 during handling and spreading. This problem was already addressed by [Hoffmeister et al.](#)  
46 [\(1964\)](#). When fertiliser is applied with a centrifugal spreader, the differences in physical  
47 properties can affect the granule behaviour during the ballistic flight. Then, ballistic  
48 segregation can occur and yield heterogeneous spatial distribution of chemical elements.  
49 Several works have examined the ballistic segregation of blended fertilisers by carrying out

1 field experiments ([Miserque and Pirard, 2004](#); [Tissot et al., 1999](#); [Virk et al., 2013](#)). All these  
2 studies required huge field test to evaluate the mass and nutrient distribution.  
3 In order to circumvent cumbersome experiments or reduce the number of experiments, some  
4 author attempted to develop new approaches based on modeling fertiliser granule motion.  
5 Recently, [Antille et al. \(2013\)](#) suggested the particle size range of new fertilisers could be  
6 designed to meet a target bout width and the author proposed to model and simulate the  
7 ballistic flight to assess whether granule physical properties suited the spreading objective.  
8 [Grafton et al. \(2015\)](#) also suggested the use of a ballistic model to provide information to  
9 reduce the risk of crop striping. In these recent works, the proposed models were limited to  
10 predict the landing distance of some individual granules projected by a spinning disc.  
11 Therefore, no spread pattern was computed so that no transverse distribution can be  
12 determined.

13  
14 Numerous works have attempted to model the motion of fertiliser granules in the spreading  
15 process. Various mechanical models have been proposed to describe the motion of individual  
16 fertiliser granules on a spinner disc ([Cunningham, 1963](#); [Cunningham and Chao, 1967](#);  
17 [Hofstee, 1995](#); [Inns and Reece, 1962](#); [Olieslagers, 1997](#); [Patterson and Reece, 1962](#); [Villette  
18 et al., 2005](#)) and through the air ([Antille et al., 2015](#); [Mennel and Reece, 1963](#); [Pitt et al.,  
19 1982](#)). Concerning the motion on the disc, models using the discrete element method (DEM)  
20 have also been developed to take into account particle interactions ([Casas et al., 2015](#);  
21 [Coetzee and Lombard, 2011](#); [Tijskens et al., 2005](#); [Van Liedekerke et al., 2006](#)). One  
22 drawback of DEM models is that they required input parameters that are difficult to obtain to  
23 characterise the physical behaviour of fertilisers. When results of simulations are compared  
24 with actual spread pattern depositions, they reach moderate success even when spreading  
25 distances are lower than 3m ([Coetzee and Lombard, 2011](#); [Van Liedekerke et al., 2009](#)).  
26 Consequently, at the present time, no model appears sufficiently advanced to correctly  
27 simulate actual spread pattern depositions. Moreover, to the best of our knowledge, no model  
28 reproduces the random variability observed from run to run in spreader test.

29  
30 Despite some experimental studies, the comparison of spreader transverse tests using different  
31 collection trays or different test protocols is still difficult and the main conclusion is limited to  
32 the recommendation of using the same test to give sense to comparisons. For example, there is  
33 a lack of knowledge concerning the quantitative effect of the surface or shape of collection  
34 trays on the CV measurement. Similarly, the effect on the CV of increasing the number of  
35 runs or reducing the speed travel of some standard tests has not been studied. In addition, the  
36 effect of the application rate on the measurement of the CV value has never been studied. This  
37 lack of information results from the difficulty, not to say impossibility, of carrying out  
38 adapted experiments with enough replications. The same difficulty limited the production of  
39 knowledge on the spatial distribution of fertiliser particle size and on the ballistic segregation  
40 for blended fertilisers. An alternative solution lies in the use of models to simulate the  
41 physical phenomena and carry out in silico experimental studies. The main advantages of this  
42 approach are to avoid practical and time limitations so that statistical parameters can be  
43 deduced from replications. Nevertheless, this implies that simulation models have to  
44 reproduce the stochastic nature of fertiliser dispersal processes.

45 The aim of this paper is to design such a model for simulating realistic fertiliser spread  
46 patterns and providing new solutions to carry out numerical experiments. This hybrid model  
47 combines a mechanistic approach based on the use of mechanical relationships and a  
48 stochastic approach based on the use of the statistical distributions of input parameters. The  
49 simulation model is used to study the sense of the CV value deduced from transverse tests  
50 according to the target application rate and the test method. The paper also presents an insight

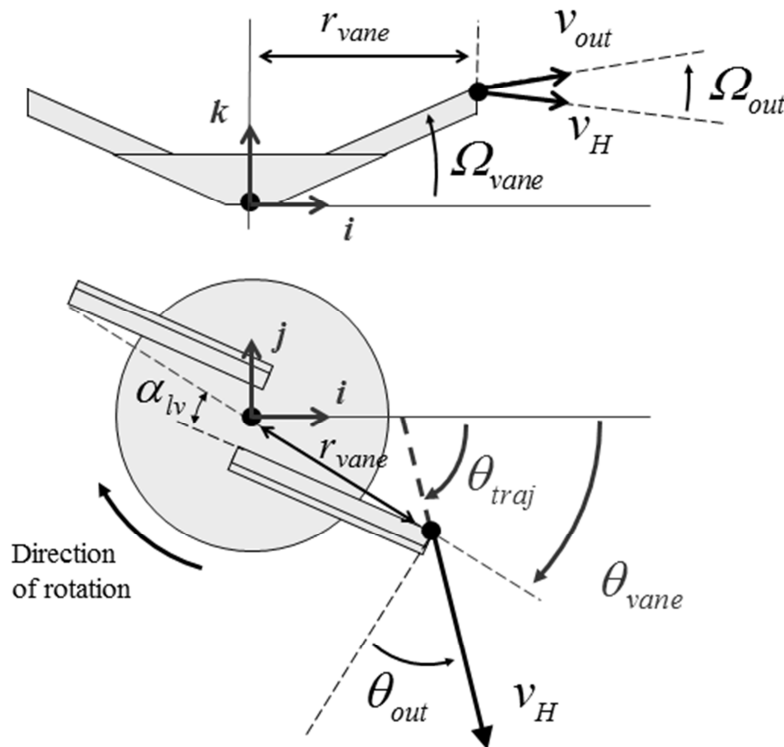
1 into the influence of particle size distributions and particle drag coefficients on transverse  
 2 distributions.

## 3 4 5 **2. Materials and methods**

6  
7 The particularity of the Hybrid Centrifugal Spreading Model HCSM lies in combining some  
 8 theoretical motion models with experimental data obtained at various steps of the spreading  
 9 process. This model assumes the spread pattern deposition is affected by the outlet velocity of  
 10 the particles when they leave the spinning disc, the angular mass flow distribution around the  
 11 disc and the fertiliser particle properties (specific density, size-distribution, drag coefficient).  
 12

### 13 **2.1 Model of granule motion on and off the spinning disc**

14  
15 Concerning the motion of the granules on the spinning disc, the HCSM considers the  
 16 kinematic relationships between the disc configuration, the outlet angles and the outlet  
 17 velocity components. In this section, the motion model is described for a clockwise spinning  
 18 disc. Figure 1 presents the main geometrical parameters used to describe the disc and the  
 19 motion of the granules when they leave the vane.



20  
21 Fig. 1 - Side view (top) and top view (bottom) of a clockwise spinning disc:  $v_{out}$ , outlet  
 22 velocity;  $v_H$ , horizontal component of the outlet velocity;  $\theta_{out}$ , horizontal outlet angle;  $\theta_{traj}$ ,  
 23 horizontal angle of the trajectory;  $\Omega_{out}$ , vertical outlet angle;  $r_{vane}$ , radius of the vane;  $\alpha_{lv}$ , pitch  
 24 angle of the vane;  $i, j, k$ , vectors of a right handed Cartesian coordinate system centred on the  
 25 disc axle.

26  
27 Let  $(O, i, j, k)$  be a three dimensional right-handed Cartesian coordinate system having its  
 28 origin  $O$  on the rotational axle of the disc and with  $j$  pointing in the travel direction.

29 In this coordinate system, the location  $(x_{out}, y_{out}, z_{out})$  of the granule when it leaves the vane is:

$$\begin{cases} x_{out} = r_{vane} \times \cos \theta_{vane} \\ y_{out} = r_{vane} \times \sin \theta_{vane} \\ z_{out} = h_{vane} \end{cases} \quad (1)$$

where  $r_{vane}$  is the radius of the vane,  $\theta_{vane}$  is the angular location of the vane,  $h_{vane}$  is the height of the outer extremity of the vane.

For a concave disc, the relationship between the vertical outlet angle  $\Omega_{out}$  of the particle when it leaves the vane, the horizontal outlet angle  $\theta_{out}$ , the vertical angle of the vane  $\Omega_{vane}$  and the pitch angle of the vane  $\alpha_{lv}$ , is as follows:

$$\Omega_{out} = \arctan \left( \frac{\sin \theta_{out} \tan \Omega_{vane}}{\cos \alpha_{lv}} \right) \quad (2)$$

The horizontal component of the outlet velocity is also deduced from  $\theta_{out}$  as follows:

$$v_H = \frac{r_{vane} \omega}{\cos \theta_{out} + \sin \theta_{out} \tan \alpha_{lv}} \quad (3)$$

where  $\omega$  is the rotational speed of the disc.

Demonstrations of equations (2) and (3) can be found in [Villette et al. \(2008\)](#).

Then, the outlet velocity is deduced:

$$v_{out} = \frac{v_H}{\cos \Omega_{out}} \quad (4)$$

According to Fig. 1, for a clockwise rotating disc, the expression of the horizontal orientation  $\theta_{traj}$  of the outlet velocity with respect to  $\mathbf{i}$  is as follows:

$$\theta_{traj} = \theta_{vane} + \theta_{out} - 90^\circ \quad (5)$$

The components of the outlet velocity in the Cartesian coordinate system (O,  $\mathbf{i}$ ,  $\mathbf{j}$ ,  $\mathbf{k}$ ) are:

$$\begin{cases} vx_{out} = v_H \times \cos \theta_{traj} \\ vy_{out} = v_H \times \sin \theta_{traj} \\ vz_{out} = v_{out} \times \sin \Omega_{out} \end{cases} \quad (6)$$

In this model, owing to Eq. (2), the vertical outlet angle is not taken as the vertical angle of the vane unlike some other models suggested in the literature ([Gomez-Gil et al., 2009](#); [Olieslagers et al., 1996](#)). This avoids coarse approximations in computing the initial conditions of the ballistic flight.

During the ballistic flight the model considers that the forces acting on the granule are only the gravity force and the drag force due to the motion of the granule through immobile air. This simple ballistic model had been used in numerous works such as [Mennel and Reece \(1963\)](#), [Pitt et al. \(1982\)](#), [Griffis et al. \(1983\)](#), [Olieslagers et al. \(1996\)](#), [Grift and Hofstee \(2002\)](#), [Reumers et al. \(2003\)](#), [Aphale et al. \(2003\)](#), [Bradley and Farnish \(2005\)](#). In the three dimensional Cartesian coordinate system, the motion in the air is described by the following differential equations:

$$\begin{cases} \frac{d^2x}{dt^2} = -K_a vx \sqrt{vx^2 + vy^2 + vz^2} \\ \frac{d^2y}{dt^2} = -K_a vy \sqrt{vx^2 + vy^2 + vz^2} \\ \frac{d^2z}{dt^2} = -g - K_a vz \sqrt{vx^2 + vy^2 + vz^2} \end{cases} \quad (7)$$

1 where  $x, y, z$  are the coordinates of the granule;  $v_x, v_y, v_z$  are the velocity components of the  
2 granule,  $g$  is the acceleration due to gravity and  $K_a$  is as follows:

$$3 \quad K_a = \frac{1}{2m} C_d A_p \rho_{air} \quad (8)$$

4 where  $m$  is the granule mass,  $C_d$  is the drag coefficient,  $A_p$  is the projected surface area of the  
5 granule,  $\rho_{air}$  is the air density. In this study,  $A_p$  is computed for spherical shapes.

## 7 **2.2 Spreading process parameters**

9 The HCSM uses experimental data measured at the beginning and at the end of the ballistic  
10 flight. This provides the initial parameters of the ballistic flight (i.e. outlet velocity) but also  
11 makes possible the estimation of the drag coefficient during the flight. The combination of  
12 these experimental measurements with mechanical models is of particular interest to take into  
13 account the actual behaviour of the fertiliser in the spreading process ([Grift et al., 2006](#);  
14 [Reumers et al., 2003](#)) and to provide realistic simulations.

15 In the spreading simulations, the motion of a high number of fertiliser granules is computed.  
16 To compute one simulation some variables are taken constant for all granules while some  
17 other variables assign random values for each granule. These last variables are associated with  
18 certain probability distributions. Thus, some probability distribution functions or the  
19 corresponding cumulative distribution functions needs to be defined.

20 This section describes the input parameters used in the simulations and their measurement  
21 methods.

### 23 2.2.1 Experimental spreading device and spread pattern deposition

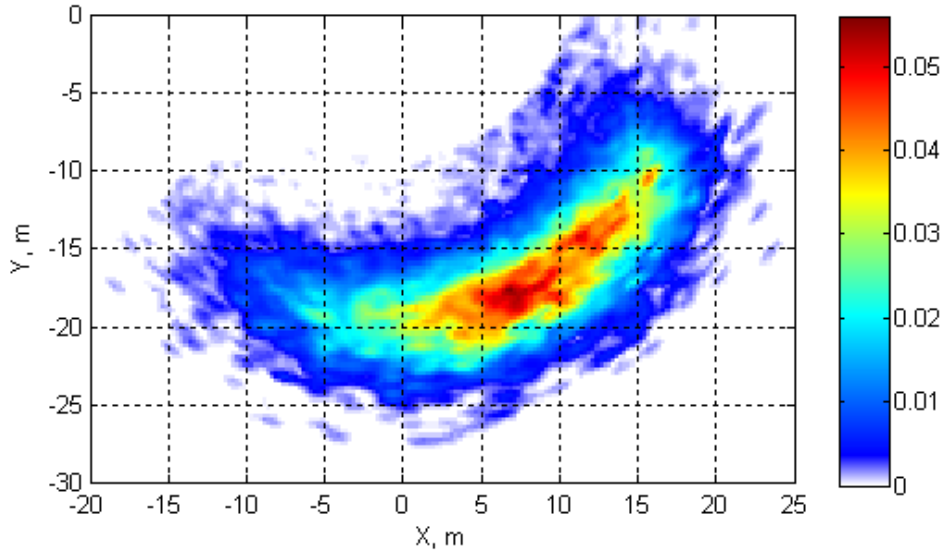
25 A custom-made spreader was used for the experimental measurements. This spreader  
26 consisted of a single clockwise rotating disc. This concave disc was equipped with two radial  
27 vanes ( $\Omega_{vane}$  was  $13.5^\circ$ ;  $\alpha_{iv}$  was  $0^\circ$ ;  $r_{vane}$  was 0.395 m) and was spinning at 810 rpm. The  
28 height  $h_{vane}$  of the outer extremity of the vanes was 0.8 m. The feeding mass flow was 0.97  
29 kg/s.

30 The stationary spread pattern obtained with this spreader and with ammonium nitrate was  
31 measured using a rotating test bench called CEMIB. This measurement device consisted in a  
32 rotating carrier and a motionless line of 80 collection trays. Each tray was equipped of a load  
33 cell and had a square collection area of  $0.5 \times 0.5$  m. The design and the advantages of this test  
34 bench are detailed in [Piron and Miclet \(2005\)](#) and [Piron et al. \(2010\)](#).

35 During the spreading, the spreader carrier turned at a constant rotation speed of  $3.1^\circ/s$ , so that  
36 the whole spread pattern passed above the collection tray row. During the rotation, the  
37 cumulated mass collected by each tray was recorded and the weight values were stored with  
38 the corresponding orientation angle of the carrier, measured by an angular optical encoder.  
39 The acquisition frequency was 10 Hz. During the whole carrier rotation, the total fertiliser  
40 mass ejected by the spreader was approximately 38 kg and the total mass collected by all the  
41 trays was approximately 0.45 kg.

42 Using this measurement device, the resulting raw data was a matrix where each line  
43 corresponded to an orientation angle and each column corresponded to the cumulative  
44 fertiliser mass collected in each tray. The fertiliser mass collected at each angular location was  
45 then derived from cumulative measurements. Since the collection areas of all trays are the  
46 same, the spatial density of the fertiliser deposition was directly deduced from previous data  
47 in polar coordinates. Then, the spread pattern deposition was computed by the CEMIB  
48 algorithm, with respect to the disc centre in Cartesian coordinates, using a mathematical  
49 interpolation and a sampling interval of  $0.25 \times 0.25$  m. Figure 2 presents the spread pattern

1 deposition obtained with the experimental spreader and the ammonium nitrate fertiliser used  
 2 in this study. This spread pattern is taken as reference data for the study.  
 3 The analysis of the spread pattern deposition shows that the mean radius of the spread pattern  
 4 slightly increases with the rotation of the vane (i.e. from the beginning to the end of the  
 5 spreading angular sector).



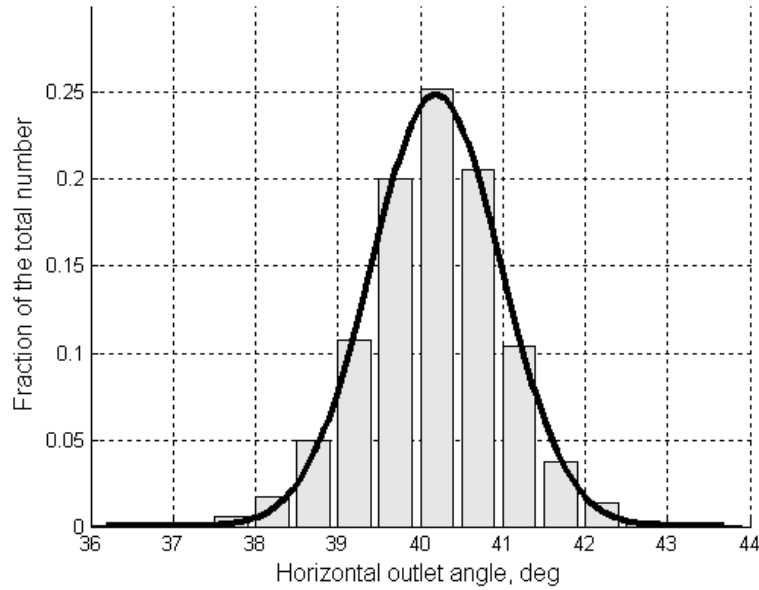
6  
 7 Fig. 2 - Stationary spread pattern obtained for ammonium nitrate and the experimental  
 8 spreader. The graduation of the colour scale reflects the fertiliser amount lying on the  
 9 sampling area (0.25×0.25 m) expressed in percentage of the total mass.

10  
 11 2.2.2 Horizontal outlet angle distribution

12  
 13 The horizontal outlet angles  $\theta_{out}$  were measured using an imaging system based on the  
 14 processing of motion-blurred images. In this acquisition technique, the exposure time is long  
 15 relative to the velocity of fertiliser granules so that the granule displacements appear as  
 16 streaks across the image. The horizontal outlet angles were derived from the distance between  
 17 these streaks and the disc axle. The imaging system and the image processing are detailed in  
 18 [Villette et al. \(2008\)](#).

19 Images were captured with a monochrome CCD camera (Sony XCD-SX910), equipped with a  
 20 6 mm lens. The camera was approximately placed at 0.7 m above the upper corner of the vane  
 21 and approximately above the central part of the spreading angular sector. The optical axis of  
 22 the camera was set parallel to the disc axle at a distance of approximately 0.5 m from this  
 23 axle. Using a set of 300 images, the horizontal outlet angle was measured for trajectories  
 24 selected near the principal point of the image (i.e. the point corresponding to the view axis in  
 25 the image) to improve the measurement accuracy and avoid geometrical bias. Thus, 2280  
 26 trajectories lying in a 10° spreading angular sector were used to estimate the horizontal outlet  
 27 angle. The angular location of the vane  $\theta_{vane}$  corresponding to the middle of this sector was -  
 28 20°. The mean value  $\mu\theta_{out}$  was 40.2° and the standard deviation  $\sigma\theta_{out}$  was 0.85°.

29 Considering the histogram of the measured value (Fig. 3), the probability density function was  
 30 chosen as a normal distribution defined by the two parameters:  $\mu\theta_{out}$  and  $\sigma\theta_{out}$ .



1  
2 Fig. 3 - Distribution histogram of the horizontal outlet angle measured in the middle of the  
3 spreading angular sector. The Gaussian curve that fits the distribution is superposed  
4 (continuous line).

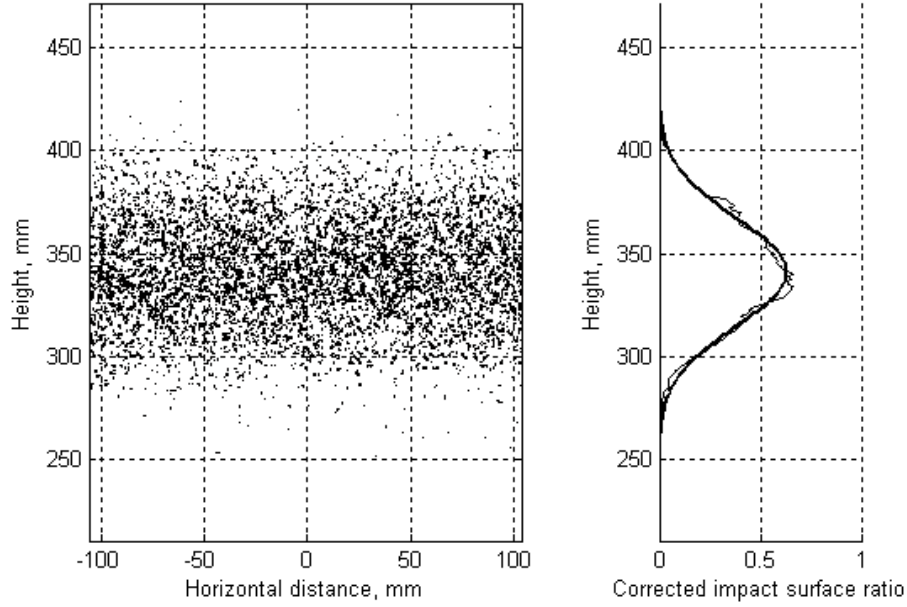
5  
6 In order to take into account, the slight increase of the spread pattern radius with respect to the  
7 rotation of the vane, the mean value  $\mu\theta_{out}$  was modelled by the following linear relationship:

$$8 \quad \mu\theta_{out} = 39.2 - 0.05 \times \theta_{vane} \quad (9)$$

9 where  $\mu\theta_{out}$  and  $\theta_{vane}$  are expressed in degrees.

### 10 11 2.2.3 Vertical outlet angle distribution

12  
13 For a given value of the horizontal outlet angle  $\theta_{out}$ , the mean value of the corresponding  
14 vertical outlet angle  $\Omega_{out}$  was provided by Eq. (2). Nevertheless, this relationship did not  
15 model the dispersion of  $\Omega_{out}$  around its mean value. Consequently this dispersion was  
16 measured separately by analysing the vertical distribution of the mass flow. The experimental  
17 method consisted in recording granule impacts on a vertical screen placed in the vicinity of  
18 the spinning disc. The method is the same than the one described in [Villette et al. \(2013\)](#),  
19 except a simple flat screen was used instead of a cylindrical screen. Moreover a shutter  
20 system was added to control the exposure time of the screen to fertiliser impacts. The screen  
21 was covered with a paper of A4 size, a carbon film and a protective film, so that granules  
22 hitting the screen produced impact marks on the recording paper (Fig. 4). After the exposition  
23 of the recording paper to granule shocks, the paper was digitalised and a dedicated image  
24 processing was carried out to analyse the vertical distribution of the impacts. The details of  
25 the mathematical model and algorithms used to process impact records or compute the  
26 corrected impact surface ratio, can be found in [Villette et al. \(2013\)](#). Considering the curve of  
27 the vertical distribution of the impacts (Fig. 4), the probability density function was chosen as  
28 a normal distribution. Placing the recording screen at 1.08 m and 2.09 m from the axle of the  
29 spinning disc, 5 replications of impact recording were carried out at each distance. The mean  
30 values of the standard deviations of the impact heights were respectively: 13.3 mm and 25.9  
31 mm. Then, the standard deviation  $\sigma\Omega_{out}$  of the vertical outlet angle was estimated at 0.7°.



1  
2 Fig. 4 - Example of impact record (left) and the corresponding vertical impact distribution  
3 (right) expressed in terms of corrected impact surface ratio. The Gaussian curve (bold) that  
4 fits the distribution is superposed.

#### 6 2.2.4 Angular mass flow distribution

7  
8 The angular mass flow distribution was computed at the outer extremity of the vane, as a  
9 function of the angular location of the vane. The distribution was deduced from the spread  
10 pattern deposition and the horizontal outlet angle. The whole spreading angular sector was  
11 sampled each degree. For each angular location of the vane, the theoretical horizontal  
12 direction was computed using Eq. (5) and the relative fertiliser quantity was computed for  
13 each sampled angular sector from the outer extremity of the vane to a range of 30 m with a  
14 sampling interval of 0.25 m. Thus, the spread pattern deposition was computed as a function  
15 of the spreading distance (from the extremity of the vane to the landing point) and the angular  
16 location of the vane (Fig. 5). The angular mass flow distribution  $g_M(\theta_{vane})$  at the extremity of  
17 the vane (Fig. 5) was obtained by summing the relative mass of fertiliser obtained for each  
18 vane location (whatever the spreading distance). The cumulative mass flow distribution with  
19 respect to the vane location  $G_M(\theta_{vane})$  was deduced from  $g_M(\theta_{vane})$  as follows:

$$20 \quad G_M(\theta_{vane}) = \int_{-\infty}^{\theta_{vane}} g_M(\xi) d\xi \quad (10)$$

21 This distribution was used in the HCSM to compute the probability of the fertiliser mass  
22 ejected for each angular position of the vane for the clockwise spinning disc of the virtual  
23 spreader.  
24

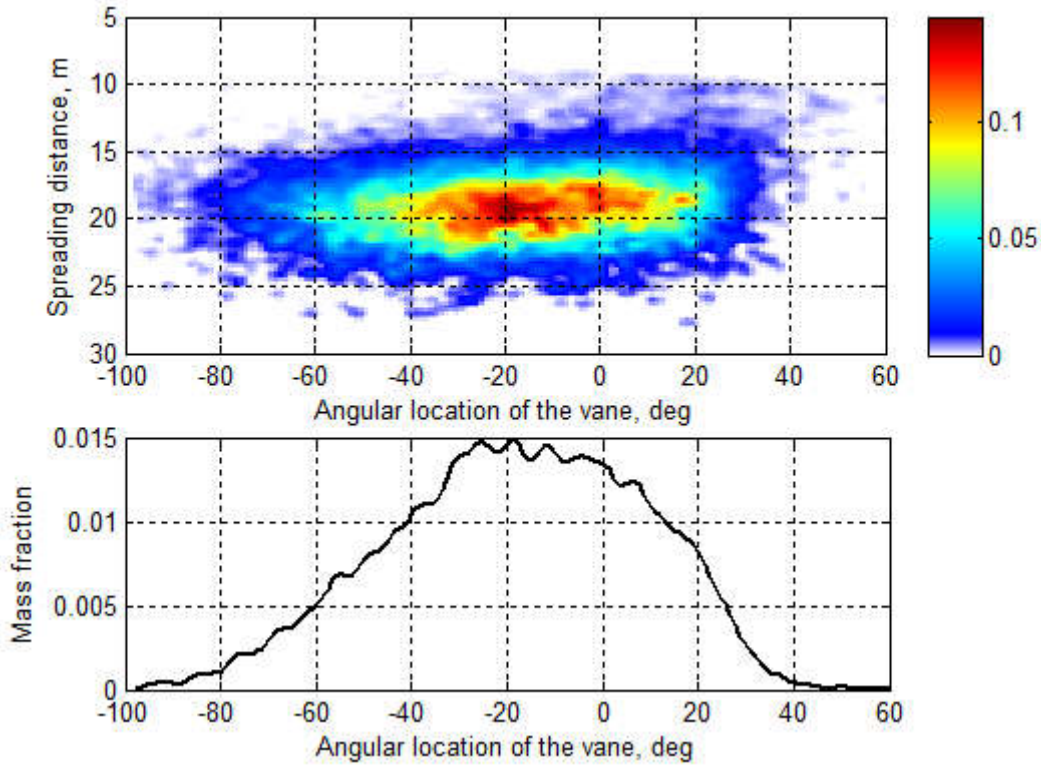


Fig. 5 - Spread pattern deposition (top) and angular distribution of the mass flow (bottom). The spread pattern deposition is drawn as a function of the spreading distance and the angular location of the vane. The graduation of the colour scale reflects the fertiliser amount lying on the sampling area ( $0.25 \text{ m} \times 1^\circ$ ), expressed in percentage of the total mass.

## 2.3 Fertiliser parameters

In this study, ammonium nitrate was used for actual experiments. The same fertiliser characteristics were used in numerical simulations computed with the HSCM. The shape of the granules was assumed to be spherical.

### 2.3.1 Specific density

The density of the fertiliser granules was deduced from weighing a material bulk volume and weighing anew the same bulk volume after completing with a liquid of known density. Then, the volume of the granules is deduced and the granule density is calculated. For the ammonium nitrate used in this study, the specific density  $\rho$  was  $1563 \text{ kg.m}^{-3}$ .

### 2.3.2 Granule diameter distribution

The particle size analysis was performed with a sieving test according to the European standard EN 1235/A1 (2003). This provided the cumulative mass distribution function. Then, a two-parameter lognormal distribution was used to describe the distribution.

Thus, the normalised cumulative mass distribution (value range from 0 to 1) was fit with the following function:

$$G_D(d_p) = \frac{1}{2} + \frac{1}{2} \operatorname{erf} \left( \frac{\ln(d_p) - \mu_{ln}}{\sqrt{2}\sigma_{ln}} \right) \quad (11)$$

1 where  $d_p$  is the granule diameter, erf() is the error function,  $\mu_m$  and  $\sigma_m$  are the two fitting  
 2 parameters (corresponding to the mean and standard deviation of the variable's natural  
 3 logarithm).

4 The derivative function of  $G_D(d_p)$  is:

$$5 \quad g_D(d_p) = \frac{1}{d_p \sigma_m \sqrt{2\pi}} \exp\left(-\frac{(\ln(d_p) - \mu_m)^2}{2\sigma_m^2}\right) \quad (12)$$

6 Considering the probability density function  $f_D(d_p)$  and the cumulative frequency function  
 7  $F_D(d_p)$  of the random variable  $D$ , the probability of having the granule diameter  $D$  lower than  
 8  $d_p$  is:

$$9 \quad p(\{D \leq d_p\}) = F_D(d_p) = \int_0^{d_p} f_D(\xi) d\xi \quad (13)$$

10 Using the probability density function  $f_D(d_p)$ , the cumulative mass distribution  $G_D(d_p)$  is also  
 11 expressed as follows:

$$12 \quad G_D(d_p) = \frac{\int_0^{d_p} f_D(\xi) \times m(\xi) d\xi}{\int_0^{+\infty} f_D(\xi) \times m(\xi) d\xi} \quad (14)$$

13 where  $m(d_p)$  is the mass of granules of diameter  $d_p$ .

14 Assuming the mass of the granule is proportional to  $d_p^3$ , Eq. (14) yields:

$$15 \quad G_D(d_p) = \frac{1}{K} \int_0^{d_p} f_D(\xi) \times \xi^3 d\xi \quad (15)$$

16 where  $K = \int_0^{+\infty} f_D(\xi) \times \xi^3 d\xi$

17 This provides:

$$18 \quad g_D(d_p) = \frac{1}{K} f_D(d_p) \times d_p^3 \quad (16)$$

19 Combining Eq. (13) and Eq. (16), the cumulative frequency function of the granule diameter  
 20 is finally obtained as follows:

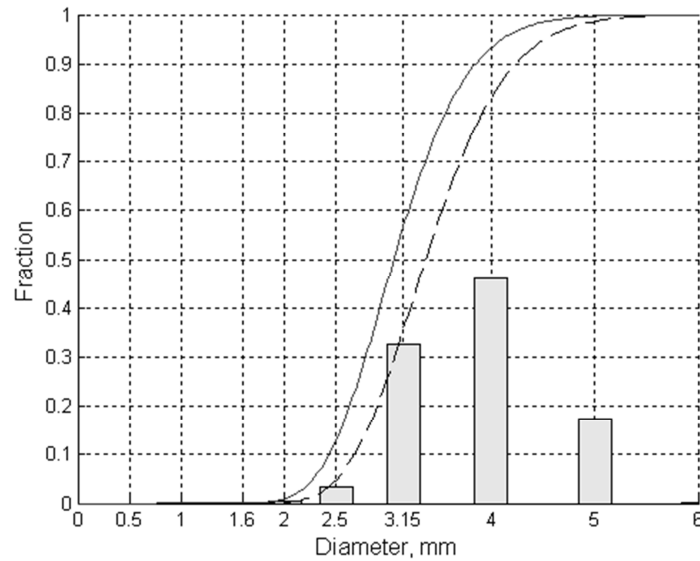
$$21 \quad F_D(d_p) = K \int_0^{d_p} \frac{g_D(\xi)}{\xi^3} d\xi \quad (17)$$

22 In practice, the integration of Eq. (17) is computed numerically and the constant  $K$  is  
 23 determined so that  $F_D(d_p)$  is 1 when  $d_p$  tends to infinity.

24

25 For the ammonium nitrate fertiliser used in this study, Fig. 6 presents the results of the sieve  
 26 test with the corresponding cumulative mass distribution  $G_D(d_p)$  and the cumulative frequency  
 27 function  $F_D(d_p)$ .

28



1  
2 Fig. 6 - Results of the particle size analysis: fraction of the fertiliser mass retained on each  
3 sieve (bar graph), cumulative mass distribution  $G_D(d_p)$  (dashed line), cumulative frequency  
4 function  $F_D(d_p)$  (continuous line).

5  
6 The establishment of the cumulative frequency function  $F_D(d_p)$  is of particular interest to  
7 select efficiently random diameter values corresponding to a random set of granules whose  
8 the mass distribution respects the fertiliser sieve test.

### 9 10 2.3.3 Drag coefficient in the air

11  
12 To compute the ballistic flight of fertiliser particles, many researchers assumed the drag  
13 coefficient  $C_d$  to be constant ([Coetzee and Lombard, 2011](#); [Grafton et al., 2015](#); [Grift and](#)  
14 [Hofstee, 2002](#); [Olieslagers et al., 1996](#); [Pitt et al., 1982](#)), while some other authors tried to  
15 improve the description of the ballistic flight by considering changes of the  $C_d$  value during  
16 the motion ([Antille et al., 2015](#)).

17 In some works, the fertiliser particles were approximated as perfect spheres. Consequently,  
18 considering a turbulent flow regime, the  $C_d$  value of the fertiliser granules was chosen at 0.44  
19 ([Coetzee and Lombard, 2011](#); [Olieslagers et al., 1996](#); [Walker et al., 1997](#)). Taking into  
20 account the influence of shape and texture of fertiliser granules on their aerodynamic  
21 behaviour, some other authors chose higher  $C_d$  values. For instance, [Pitt et al. \(1982\)](#) chose  
22 0.46 for ammonium nitrate. Comparing modelled and measured fall time, [Grift and Hofstee](#)  
23 [\(2002\)](#) suggested multiplying the diameter of the equivalent sphere by a correction factor  
24 (named “q-factor”) ranged from 0 to 1.

25 In the present study, the drag coefficient was assumed constant during the ballistic flight. The  
26 value of  $C_d$  was chosen by comparing the reference spread pattern (i.e. obtained with the  
27 CEMIB test bench) with simulated spread patterns computed for various  $C_d$  values. Thus, for  
28 the ammonium nitrate used in this study, the value of the drag coefficient was estimated to  
29 0.47. Moreover, the air density  $\rho_{air}$  was assumed to be  $1.21 \text{ kg/m}^3$  in the spreading condition.

## 30 31 **2.4 Monte Carlo Spreading Simulation**

### 32 33 2.4.1 The virtual spreader

34  
35 The virtual spreader considered for the simulations was a twin disc spreader for which the  
36 spacing between the two disc axles  $s_{disc}$  was 1 m. Both discs had the same angular speed. The

1 right disc rotated in the counter-clockwise direction while the left one rotated in the clockwise  
 2 direction. Each disc of the spreader was fed by the same mass flow of fertiliser.  
 3 The setting of the virtual spreader consisted in modifying the angular location of the feeding  
 4 point on each disc. With this setting mechanism, rotating the angular location of  $\alpha_{set}$  for the  
 5 left disc involves the rotation of the left spread pattern in the same direction and with the same  
 6 angle  $\alpha_{set}$ .

#### 8 2.4.2 Static spread pattern simulation

10 Considering the virtual spreader, static spread patterns were computed using the HCSM and a  
 11 Monte Carlo process. This approach consisted in computing the motion of a high number of  
 12 fertiliser granules for which several characteristics were randomly drawn from pre-established  
 13 statistical distributions. Simulations were implemented with [Matlab \(2005\)](#), and used the  
 14 random number generator of this software. For normally distributed variables, the values were  
 15 obtained using the *randn* function. In the case of other arbitrary distributions, the selection of  
 16 random values was performed in two steps. First, random numbers were generated with a  
 17 uniform distribution using the *rand* function on the range 0 to 1. Second, final random values  
 18 were deduced from these random numbers by inverting the cumulative frequency function of  
 19 the specified distribution.

20 For a given mass  $m_{tot}$  of fertiliser, the computation of the spread pattern was decomposed in  
 21 computing the left and the right spread patterns independently. For the left disc, the Monte  
 22 Carlo simulation consisted of the following steps.

24 First, a set of virtual granules was generated by drawing a set of diameter values from the  
 25 fertiliser diameter distribution using the cumulative frequency function  $F_D$ . Then, the mass  $m_i$   
 26 of each granule was computed as follows:

$$27 \quad m_i = \rho \frac{\pi}{3} d_{pi}^3 \quad (18)$$

28 where  $d_{pi}$  is the diameter of the granule of mass  $m_i$ .

29 The total number  $n_{disc}$  of granules ejected by the disc was adjusted so that:

$$30 \quad \sum_{i=1}^{n_{disc}} m_i = \frac{m_{tot}}{2} \quad (19)$$

32 Second, the initial conditions of the ballistic flight were assigned to each granule  
 33 independently from its diameter. For each granule, the values of the different variables were  
 34 assigned as follows:

35 1) The angular location of the vane  $\theta_{vane}$  corresponding to the granule ejection was randomly  
 36 selected using the cumulative mass flow distribution  $G_D$ .

37 2) The corresponding coordinates of the ejection point  $(x_{out}, y_{out}, z_{out})$  were deduced from  $\theta_{vane}$   
 38 using Eq. (1).

39 3) The corresponding horizontal outlet angle  $\theta_{out}$  was drawn from the normal distribution  
 40 parametrized by  $\mu\theta_{out}$  and  $\sigma\theta_{out}$ , where  $\mu\theta_{out}$  was deduced from the vane location  $\theta_{vane}$  using  
 41 Eq. (9).

42 4) The corresponding vertical outlet angle  $\Omega_{out}$  was drawn from the normal distribution  
 43 parametrized by  $\mu\Omega_{out}$  and  $\sigma\Omega_{out}$ , where  $\mu\Omega_{out}$  was the vertical outlet angle deduced from  $\theta_{out}$   
 44 using Eq. (2).

45 5) The corresponding outlet velocity  $v_{out}$  and its 3D-components  $(v_{x_{out}}, v_{y_{out}}, v_{z_{out}})$  were  
 46 deduced from  $\theta_{vane}$ ,  $\theta_{out}$  and  $\Omega_{out}$  using successively Eqs. (3), (4), (5) and (6).

1 Third, the coordinates of the landing point of each granule were computed by solving Eq. (7)  
2 with the initial conditions of flight  $x_{out}$ ,  $y_{out}$ ,  $z_{out}$  and  $vx_{out}$ ,  $vy_{out}$ ,  $vz_{out}$ . Then, the setting of the  
3 spreader is taken into account by computing the coordinates of the landing points with the  
4 rotation angle  $\alpha_{set}$  around the disc axle.

5  
6 The spread pattern produced by the right disc is computed by 1) using anew the same process  
7 to generate a second spread pattern for another set of granules; 2) changing the sign of the  $x$   
8 coordinates of this second spread pattern.

9 The global spread pattern resulting from the twin-disc virtual spreader is finally deduced from  
10 the left and right spread patterns after translating the coordinates of the granules by half the  
11 disc spacing  $s_{disc}$  in the left or right direction. This global spread pattern is defined by a set of  
12 granules for which each mass and each landing position is perfectly known.

### 13 14 2.4.3 Transverse distribution

15  
16 The transverse distribution is deduced from the static spread pattern by considering a virtual  
17 row of collection trays placed continuously along a line perpendicular to the travel axis (along  
18 the  $x$ -axis) of the virtual spreader. For a given swath spacing  $L_w$ , several static spread patterns  
19 were computed and translated on the right and the left at a multiple of  $L_w$  of the central pass to  
20 reproduce the overlapping. The successive spread patterns were oriented to simulate overlaps  
21 resulting from adjacent swaths applied in alternate directions (*i.e.* back and forth mode).

22 Depending on the  $x$ -value of each granule of the spread patterns, the granules were affected to  
23 the corresponding collection trays, so that the sub-set of granules virtually collected by each  
24 tray was perfectly known in terms of granule masses and granule diameters. The transverse  
25 distribution of the fertiliser mass was obtained by summing the mass of all the granules  
26 virtually collected by each collection tray. Then, the transverse coefficient of variation CV is  
27 deduced from this mass distribution by dividing the standard deviation by the mean. In this  
28 paper the CV is expressed in percentage.

29 For a target application rate  $q_t$ , the total mass  $m_{tot}$  of fertiliser used to compute the static  
30 spread pattern was determined as the product of the application rate by the collection surface  
31 on the swath spacing. Calling  $l_{tray}$  the length of the collection trays (measured in the travel  
32 direction), the total mass  $m_{tot}$  is as follows:

$$33 \quad m_{tot} = q_t \times l_{tray} \times L_w \times 10^{-4} \quad (20)$$

## 34 35 3 Results and discussion

### 36 37 **3.1 Comparison of the measured and simulated spread pattern**

38  
39 Although the objective of the HCSM was not the perfect description of the physical  
40 phenomena of the spreading process or the perfect reproduction of the experimental spread  
41 pattern, it is important to ensure the simulated spread pattern was in accordance with  
42 experimental results. Thus, the first simulation consisted in computing the spread pattern for a  
43 single disc for the same spreading conditions than those carried out with the experimental  
44 spreading device.

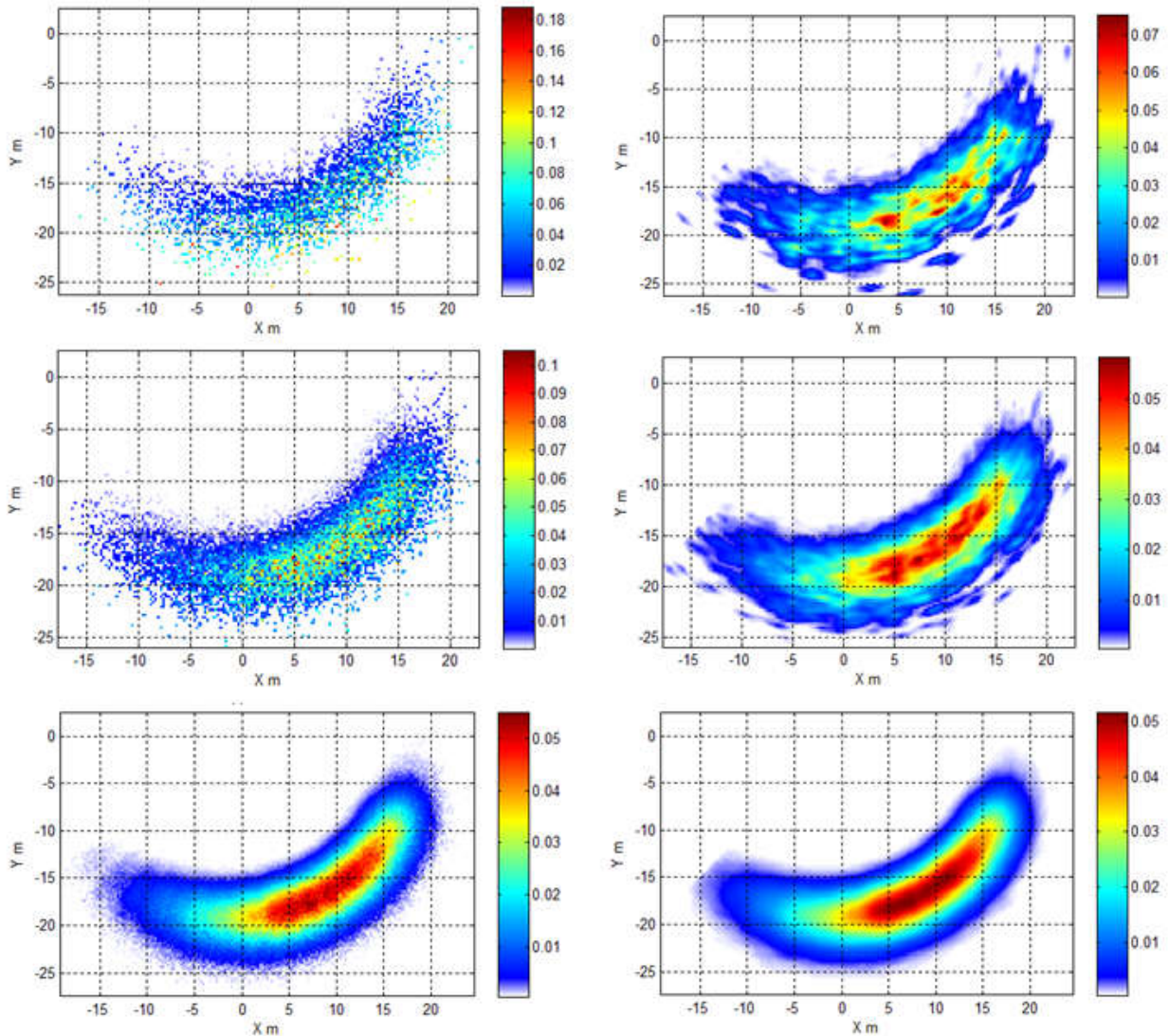
45 The 2D-representation of the spread pattern deposition was obtained by considering a grid  
46 with a sampling interval  $\Delta w_{grid} = 0.25$  m and  $\Delta l_{grid} = 0.25$  m in the transverse and longitudinal  
47 directions. Depending on the granule coordinates, the granules located in each grid cell were  
48 identified and the sum of their masses was affected to the corresponding cell. This matrix was  
49 the raw Cartesian representation of the spread pattern deposition.

1 As the experimental measurement device (CEMIB) was a rotating system, and as the  
2 processing of the polar data included some interpolation and regularization steps, it was  
3 difficult to compare visually the raw Cartesian representation of the simulated spread pattern  
4 with the interpolated experimental measurement (especially for low fertiliser amount).  
5 Thus, the raw Cartesian representations of the simulated spread pattern had been sampled in a  
6 polar coordinate system, regularized by a Gaussian filter and then re-interpolated into a  
7 Cartesian coordinate system to simulate the effect of the Cemib acquisition and data  
8 processing. For three different amount of fertiliser, Fig. 7 shows the raw Cartesian  
9 representation of the simulated spread pattern deposition and its representation when  
10 interpolations are applied in an intermediate polar system.

11 Fig. 7 shows that the local variability increases inside the spread pattern when the fertiliser  
12 amount decreases. This corresponds to the well-known random variability observed in CV  
13 measurement from run to run. Moreover, when the fertiliser amount is 0.45 kg the  
14 representation is in good accordance with the reference spread pattern (Fig. 2) measured with  
15 the rotating test bench (when the same fertiliser amount was collected). A better comparison  
16 would have been obtained by modeling the rotating acquisition system, but this was out of  
17 scope of this paper.

18 When the fertiliser amount is very high (i.e. 50 kg), the relative local variability inside the  
19 spread pattern is reduced. Then, the representations of the spread patterns are similar whatever  
20 the use of intermediate steps in a polar system or not.

21

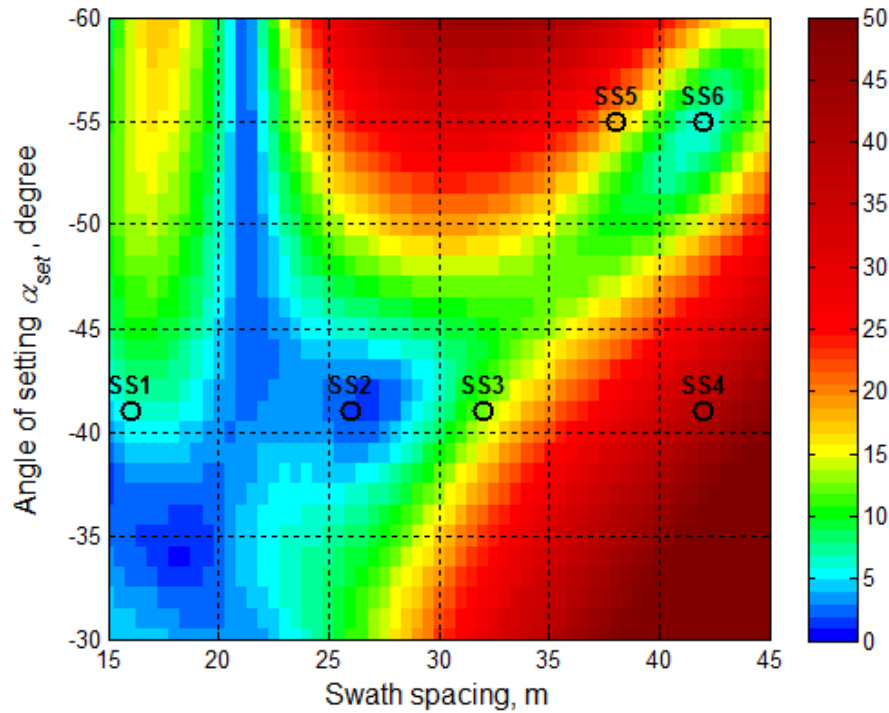


1  
 2 Fig. 7 - Simulated spread patterns for three fertiliser amounts: 0.1 kg, 0.45 kg, 50 kg (from top  
 3 to bottom) and two kind of representations: raw Cartesian representation of the simulated  
 4 spread pattern (left) and after sampling and interpolating in a polar coordinate system (right)  
 5 to reflect CEMIB data processing.  
 6

### 7 3.2 Setting map of the virtual spreader

8  
 9 A set of simulations were performed to draw the setting map of the virtual spreader. Thus, the  
 10 spread pattern was computed by considering  $10^6$  particles (i.e. a total mass of approximately  
 11 26.8 kg) ejected by each disc. The value of the setting angle was from  $-30^\circ$  to  $-60^\circ$ , and for  
 12 each value the transverse CV was computed for a set of swath spacing (from 15 to 45 m). The  
 13 size of the virtual collection trays was  $0.5 \times 0.5$  m each.

14 Figure 8 shows the setting map deduced from the simulations. This map represents the CV  
 15 value obtained with the virtual spreader with respect to setting angle and swath spacing. Since  
 16 all the CV values were computed for a very high number of particles, these values reflect the  
 17 geometry qualities or defects of the spread patterns related to the swath spacing and do not  
 18 take into account other transverse variabilities that occur for lower application rates. This CV  
 19 value is an estimation of  $CV_{geom}$  which is only due to the geometrical shape of the spread  
 20 pattern (for a specified swath spacing) regardless of the application rate.  $CV_{geom}$  is the value of  
 21 CV that would be reached if the application rate tended to infinity.



1  
2 Fig. 8 - Setting map of the virtual spreader providing the value of the CV (expressed in  
3 percentage) with respect to the setting angle and the swath spacing when the spread pattern is  
4 computed for a very high number of fertiliser granules. The color scale corresponds the value  
5 of the CV. Six specific spreading situations SS1 to SS6 are marked on the setting map (black  
6 circle).

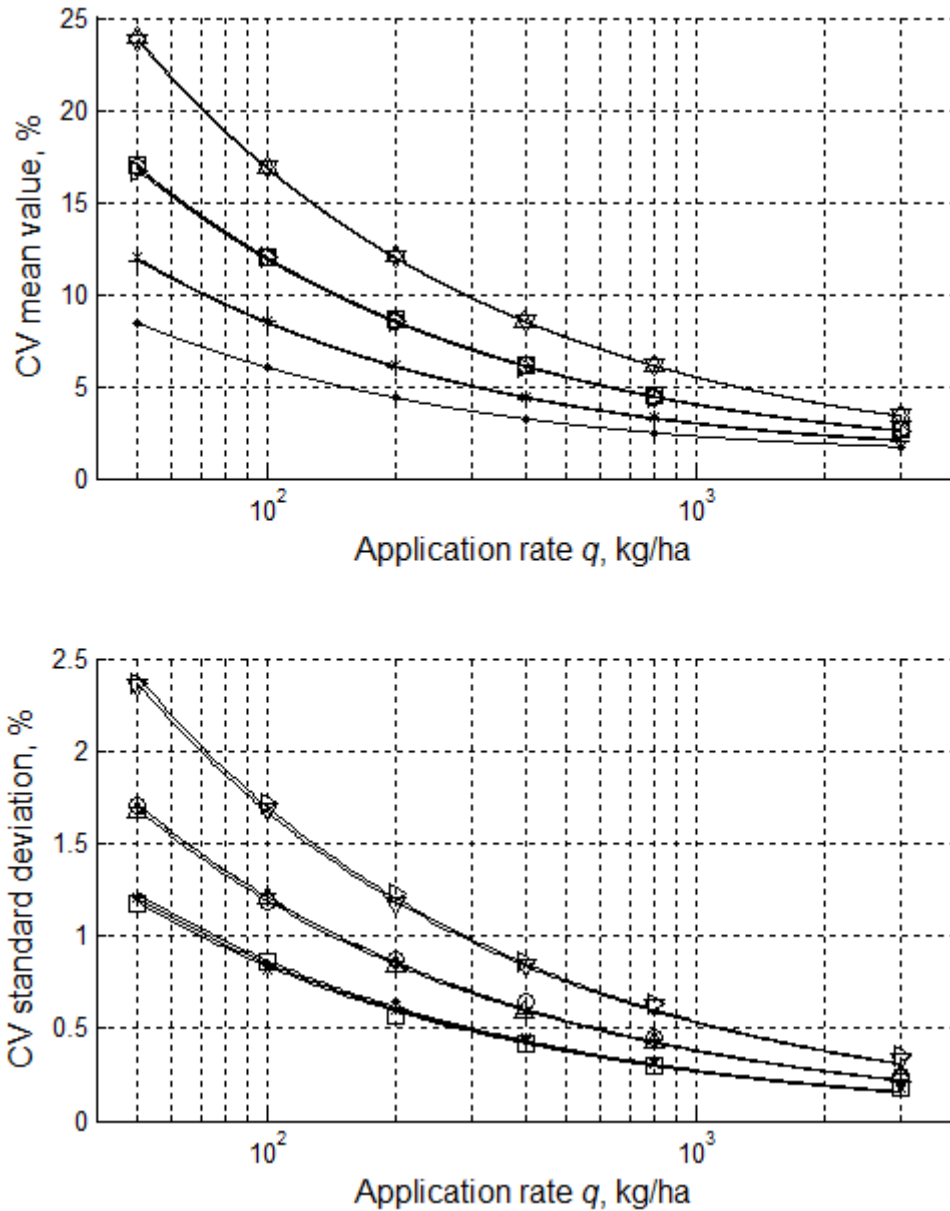
### 3.3 Influence of application rate and collection tray size on the CV value

7  
8  
9  
10 Simulations have been performed to investigate the effects of the application rate  $q$  and the  
11 collection tray size on CV measurements. For the simulations, the sizes of the collection trays  
12 (length  $\times$  width) were: 1 $\times$ 1 m, 1 $\times$ 0.5 m, 1 $\times$ 0.25 m, 0.5 $\times$ 1 m, 0.5 $\times$ 0.5 m, 0.5 $\times$ 0.25 m, 0.25 $\times$ 1  
13 m, and 0.25 $\times$ 0.5 m. The application rates were: 50, 100, 200, 400, 800, 3000 kg/ha and for  
14 each rate the number of replication runs was respectively 2000, 1000, 500, 500, 400, and 200.  
15 The simulations have been computed for six spreading situations (SS1 to SS6) located on the  
16 setting map (Fig. 8). Conditions SS1 to SS4 correspond to a setting angle of  $-41^\circ$  and swath  
17 spacing of respectively 16, 26, 32 and 42 m. Conditions SS5 and SS6 correspond to a setting  
18 angle of  $-55^\circ$  and swath spacing of respectively 36 and 42 m. These situations have been  
19 chosen to illustrate various setting conditions: optimal settings and swath spacing (SS2 and  
20 SS6) and inadequate settings or swath spacing.

21 In the case of the situation SS2, Fig. 9 demonstrates that the mean value  $\mu_{CV}$  and the standard  
22 deviation  $\sigma_{CV}$  of the CV increase when the application rate decreases. The curves also show  
23 that  $\mu_{CV}$  and  $\sigma_{CV}$  depend on the size of the collection trays. The mean value  $\mu_{CV}$  increases  
24 when the surface of the collection trays decreases, while the standard deviation  $\sigma_{CV}$  increases  
25 when the length of the collection trays decreases.

26 Concerning  $\mu_{CV}$ , as shown in Fig. 9, it appears that the values are very similar when they are  
27 deduced from simulations computed with the same tray surface. Comparing the results  
28 obtained for the six spreading situations (SS1 to SS6) at the six application rates, the  
29 maximum difference observed on the CV values is 0.36 % for the following tray dimensions  
30 1 $\times$ 0.25 m, 0.5 $\times$ 0.5 m, and 0.25 $\times$ 1 m (this maximum difference is obtained for SS4 at 200

1 kg/ha). For the dimensions 1×0.5 m and 0.5×1 m, the maximum difference is 0.24 %  
 2 (obtained for SS4 at 3000 kg/ha). For the dimensions 0.5×0.25 m and 0.25×0.5 m, the  
 3 maximum difference is 0.23 % (for SS1 at 50 kg/ha). These differences are very low  
 4 regarding the traditional range of CV values encountered in practice or regarding  $\mu_{CV}$  values  
 5 encountered here for spreading situations and all application rates (from 1.7 % to 46.3 %).  
 6 Furthermore, considering one spreading situation, the mean values of the CV obtained for all  
 7 tray size tend to converge.  
 8



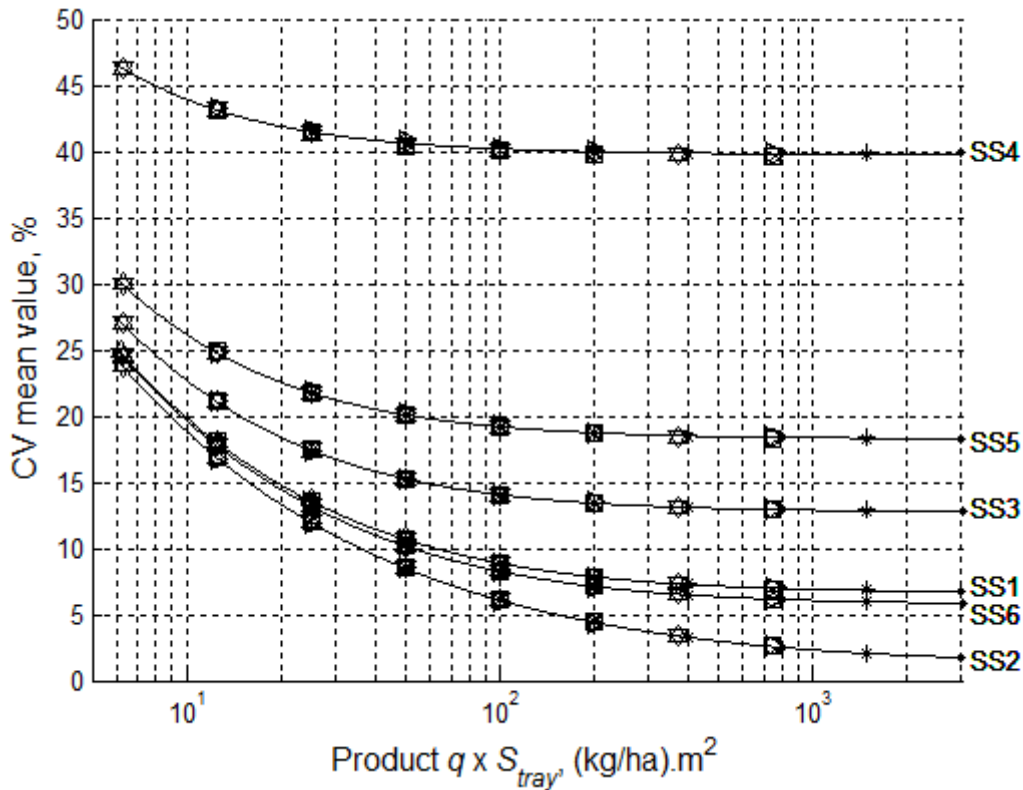
9  
 10  
 11 Fig. 9 - Mean value (top) and standard deviation (bottom) of the CV values (in %) with  
 12 respect to application rate for the spreading situation SS2 and for 8 sizes (length x width ) of  
 13 collecting trays ( • 1×1 m, □ 1×0.25 m, × 1×0.5 m, + 0.5×1 m, ○ 0.5×0.5 m, △ 0.5×0.25 m,  
 14 ▷ 0.25×1 m, ▽ 0.25×0.5 m).

15  
 16 All these observations lead to consider that the mean value of the CV depends on two  
 17 components. One component reflects the spreading situation depending on the setting and on

1 the swath spacing. This component is expressed by the constant value to which  $\mu_{CV}$  tends for  
 2 high application rates. The second component reflects the influence of the application rate  
 3 and, more precisely, the influence of the mass collected in trays (depending on the rate and  
 4 the tray surface). Consequently, the expression of the mean value of the CV is proposed as a  
 5 function of  $q$  and  $S_{tray}$  as follows:

$$6 \quad \mu_{CV} = \sqrt{\frac{a}{q \times S_{tray}} + b^2} \quad (21)$$

7 where  $q$  is expressed in kg/ha,  $S_{tray}$  is expressed in  $m^2$ ,  $a$  and  $b$  are two coefficients.  
 8 This relationship is used as a regression model to fit the data obtained for the six studied  
 9 spreading situations (SS1 to SS6). Figure 10 presents the mean value  $\mu_{CV}$  with respect to the  
 10 product of the application rate by the collection tray surface ( $q \times S_{tray}$ ). Table 1 shows the  
 11 values of the parameters  $a$ ,  $b$  and the correlation coefficient resulting from the use of Eq. (21)  
 12 to fit the data. The regression curves are drawn on Fig. 10. The values of the correlation  
 13 coefficient  $r$  demonstrate that Eq. (21) accurately describes the relationship between  $\mu_{CV}$ ,  $q$   
 14 and  $S_{tray}$ . The lowest value of correlation coefficients is obtained for SS4 but is still higher  
 15 than 0.996.



16  
 17 Fig. 10 – Mean value of the CV obtained for various spreading situations (SS1 to SS6) when  
 18 it is measured with various size of collection trays, with respect to the product of the  
 19 application rate by the collection tray surface ( $q \times S_{tray}$ ). The symbols correspond to the size  
 20 of the collection trays:  $\bullet$   $1 \times 1$  m,  $\square$   $1 \times 0.25$  m,  $\times$   $1 \times 0.5$  m,  $+$   $0.5 \times 1$  m,  $\circ$   $0.5 \times 0.5$  m,  $\triangle$   
 21  $0.5 \times 0.25$  m,  $\triangleright$   $0.25 \times 1$  m,  $\nabla$   $0.25 \times 0.5$  m.

22

1  
2  
3  
4  
5  
6  
7  
8  
9  
10  
11  
12  
13  
14  
15  
16  
17  
18  
19  
20  
21  
22  
23  
24  
25  
26  
27  
28  
29  
30  
31  
32  
33  
34  
35  
36

Table 1 – Parameters ( $a$ ,  $b$ ) and Pearson correlation coefficient ( $r$ ) of the regression model used to fit CV mean values (expressed in %) according to Eq. (21) for various spreading situations.

Spreading situation	$a$	$b$	$r$
SS1	35.1 $10^2$	6.64	0.9999
SS2	35.4 $10^2$	1.38	0.9999
SS3	35.4 $10^2$	12.74	0.9999
SS4	35.0 $10^2$	39.76	0.9969
SS5	35.2 $10^2$	18.26	0.9998
SS6	35.4 $10^2$	5.76	1.0000

Considering Eq. (21), the value of  $\mu_{CV}$  tends to  $b$  when the application rate approaches infinity. Thus, the parameter  $b$  corresponds to the  $CV_{geom}$ , which depends on the geometrical shape of the spread pattern (for a specified swath spacing) regardless of the application rate. Regarding Table 1, the values of the parameter  $a$  are very similar whatever the spreading situation. Some additional simulations shows that this value depends on the particle size distribution of the fertiliser.

Another interesting aspect of the finding expressed in Eq. (21) is that, whatever the setting of the machine, the mean value of the CV is higher than a limit defined by the application rate and the collection tray surface. This limit is as follows:

$$\mu_{CV} \geq \sqrt{\frac{a}{q \times S_{tray}}} \tag{22}$$

This means that trying to set the machine to obtain a CV below this limit does not make sense. Conversely, measuring CV values significantly higher than this value indicates that the setting or the design of the machine could be optimized to improve the spreading quality. Nevertheless, the practical use of this threshold remains dependent on the accuracy of the CV estimation regarding the measurement variability.

Concerning the standard deviation  $\sigma_{CV}$  of the CV, Fig. 9 shows that the values are close when they are deduced from simulations computed with the same collection tray length.

Comparing the results obtained for the six spreading situations (SS1 to SS6) at the six application rates, the maximum difference observed on the standard deviation is 0.25 % for the following tray dimensions 1x1 m, 1x0.25 m, 1x0.5 m. For the dimensions 0.5x1 m, 0.5x0.5 m, 0.5x0.25 m, the maximum difference is 0.19 %. For the dimensions 0.25x1 m, 0.25x0.5 m, the maximum difference is 0.2 %.

For each collection tray size and for each spreading situation, the standard deviation of the CV is well fitted by the following expression:

$$\sigma_{CV} = c(q \times l_{tray})^{-0.5} \tag{23}$$

The range of values of the parameter  $c$  and the range of value of correlation coefficients are presented in Table 2, when  $q$  is expressed in kg/ha.

1 Table 2 – Range values of parameter ( $c$ ) and Pearson correlation coefficient ( $r$ ) of the  
 2 regression model used to fit CV standard deviation values according to Eq. (23) for various  
 3 spreading situations.

Spreading situation	$c$	$r$
SS1	11.55 to 13.57	0.9893 to 0.9976
SS2	8.35 to 8.66	0.9975 to 0.9996
SS3	8.74 to 10.37	0.9914 to 0.9988
SS4	8.78 to 9.08	0.9980 to 0.9999
SS5	8.89 to 10.13	0.9900 to 0.9993
SS6	6.93 to 7.85	0.9905 to 0.9968

4  
 5 In the literature, very few studies addressed the problem of the influence of the application  
 6 rate or the collection tray size on the CV value. This is due to the difficulty in performing a  
 7 high number of replications and in maintaining constant spreading conditions to establish a  
 8 unbiased relationship when actual experiments have to be carried out.

9 Since the quality of the spreading results from numerous combined parameters, simulations  
 10 afford the possibility of, not only avoiding perturbations (e.g. humidity, wind or fertilizer  
 11 property variations) but also analyzing the studied parameter independently from the others.  
 12 This is the case in this section, where the effect of the application rate on the CV is studied  
 13 without any change in the outlet angle distribution or in the angular mass flow distribution.  
 14 This specific study is very difficult to carry out in practice, because the global shape of the  
 15 spread pattern can be modified when the feeding flow rate is modified ([Fulton et al., 2001](#))  
 16 due to the change in the feeding area on the spinning disc ([Kweon and Grift, 2006](#)), or in the  
 17 vane loading ([Villette et al., 2012](#)).

18  
 19 [Parish and de Visser \(1989\)](#) suggested that given a collection tray width  $w_1$ , and a resulting  
 20 coefficient of variation  $CV_1$ , a collection tray width of  $w_2$  will result in a new coefficient of  
 21 variation  $CV_2$ , related to  $CV_1$  as follows:

$$22 \quad \frac{CV_2}{CV_1} = \sqrt{\frac{w_1}{w_2}} \quad (24)$$

23 The length of the collection tray was implicitly the same for the two kinds of trays. The  
 24 authors underlined that, because of variability, this equation should be effective in dealing  
 25 with averages of multiple tests.

26 Using Eq.(21), the ratio of the mean value of  $CV_2$  on the mean value of  $CV_1$  is as follows:

$$27 \quad \frac{\mu_{CV_2}}{\mu_{CV_1}} = \sqrt{\frac{a \times q^{-1} \times (l \times w_2)^{-1} + CV_{geom2}^2}{a \times q^{-1} \times (l \times w_1)^{-1} + CV_{geom1}^2}} \quad (25)$$

28 where  $l$  is the length of the collection trays (which is the same for the collection trays used to  
 29 measure  $CV_1$  and  $CV_2$ ).

30 It appears that the relationship between  $CV_2$  and  $CV_1$  is more complex than the one suggested  
 31 by [Parish and de Visser \(1989\)](#) and that Eq.(24) is not correct when the geometrical  
 32 component of the CV ( $CV_{geom}$ ) is not null. Nevertheless, in the case of a good quality  
 33 spreading,  $CV_{geom1}$  and  $CV_{geom2}$  are low and are negligible compared to the component related  
 34 to the effect of the application rate. In the case of a good quality spreading, Eq.(25) yields:

$$35 \quad \frac{\mu_{CV_2}}{\mu_{CV_1}} = \sqrt{\frac{w_2^{-1}}{w_1^{-1}}} = \sqrt{\frac{w_1}{w_2}} \quad (26)$$

36 This demonstrates that the relationship proposed by [Parish and de Visser \(1989\)](#) is a correct  
 37 approximation only when the setting of the machine is very good, or when the CV value is  
 38 widely due to the effect of the application rate (low application rate).

1  
2 Simulation findings demonstrate the variability in CV measurement (i.e.  $\sigma_{CV}$ ) decreases with  
3 the application rate and the length of the collection trays used for the measurement. These  
4 results are in perfect accordance with recommendations of [Jones et al. \(2008\)](#) who concluded  
5 that multiple rows of trays, multiple passes and long trays can reduce experimental variability  
6 and improve the accuracy of bout width calculation. It is worth noting that doubling the  
7 number of passes corresponds to doubling the apparent application rate collected by the tray.  
8 Concerning the collection trays used for transverse tests, the European Standard specified in  
9 [EN 13739-2 \(2011\)](#) recommends the size (length x width ) of 0.5×0.5 m but also permits  
10 1×0.25 m. The simulation findings confirmed that the mean value expected for the CV is the  
11 same when these two collection tray sizes are used. Nevertheless, simulations demonstrates  
12 these two collection devices are not equivalent regarding the variability in CV measurement.  
13 Thus, the variability is reduced when the size of 1×0.25 m is used and the confidence in bout  
14 width calculation is improved. This illustrates that simulations would be of practical interest  
15 when standard revision process are launched.

### 16 17 **3.4 Influence of the test method on the CV value**

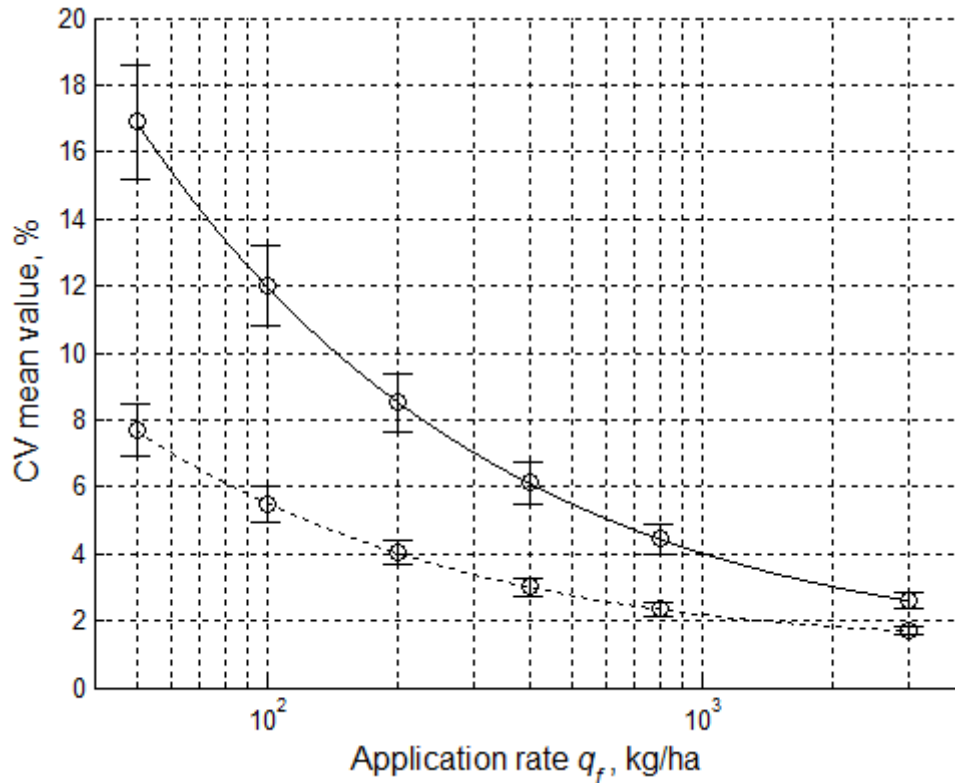
18  
19 Simulations had been carried out to compare the values of CV when they were obtained  
20 following two different measurement methods. The first method was a simple “in-field”  
21 measurement consisting in measuring the CV when the machine was driven at the forward  
22 speed of 10 km/h and was set to apply the in-field target rate  $q_f$ . The second method was a  
23 “standard test” performed following the European Standard specified in [EN 13739-2 \(2011\)](#).  
24 In this standard test, the machine was driven at 4 km/h, the number of runs for each  
25 measurement was two, and the flow adjustment using 4 km/h was set to correspond to the  
26 flow rate obtained at a forward driving speed of 10 km/h. Thus, in practice, the application  
27 rate used in the simulation program for the virtual standard test was:

$$28 \quad q = \frac{10}{4} q_f \quad (27)$$

29 Following the European Standard, two replications were done for each virtual standard test  
30 before computing the corresponding CV. Moreover, the mirror image of the transverse  
31 distribution of the central pass was used to compute the overlapped distribution with the  
32 adjacent passes on the swath spacing. In contrast, concerning the virtual “in-field”  
33 measurement, no replication is done before computing the corresponding CV and the  
34 transverse distributions for each pass were completely independent (i.e. no mirror image was  
35 used). For both test procedures, the same transverse line of collection trays was used. The size  
36 of these virtual trays was 0.5×0.5 m.

37 For the spreading situation SS2, Fig. 11 presents the mean value and error bar (twice the  
38 standard deviation) of the CV with respect to the application rate. The mean value and the  
39 standard deviation of the CV decrease with the application rate. The figure also shows that the  
40 CV is lower when it is measured with the standard procedure than when it is measured with  
41 the simple in-field test. Moreover, the standard deviation is lower when it is measured  
42 following the standard procedure (the standard deviation is approximately divided by 2).  
43 These results illustrate that the use of the standard test reduce the variability on the  
44 measurement of the CV. Nevertheless, the standard test underestimates the value of the CV  
45 with respect to the value that should be obtained in field by considering the actual target  
46 application rate (i.e. with the actual application rate at the actual forward speed and without  
47 any replication). In this example, the “in-field” CV is at least twice the “standard” CV when  
48 the application rate is lower than 490 kg/ha.

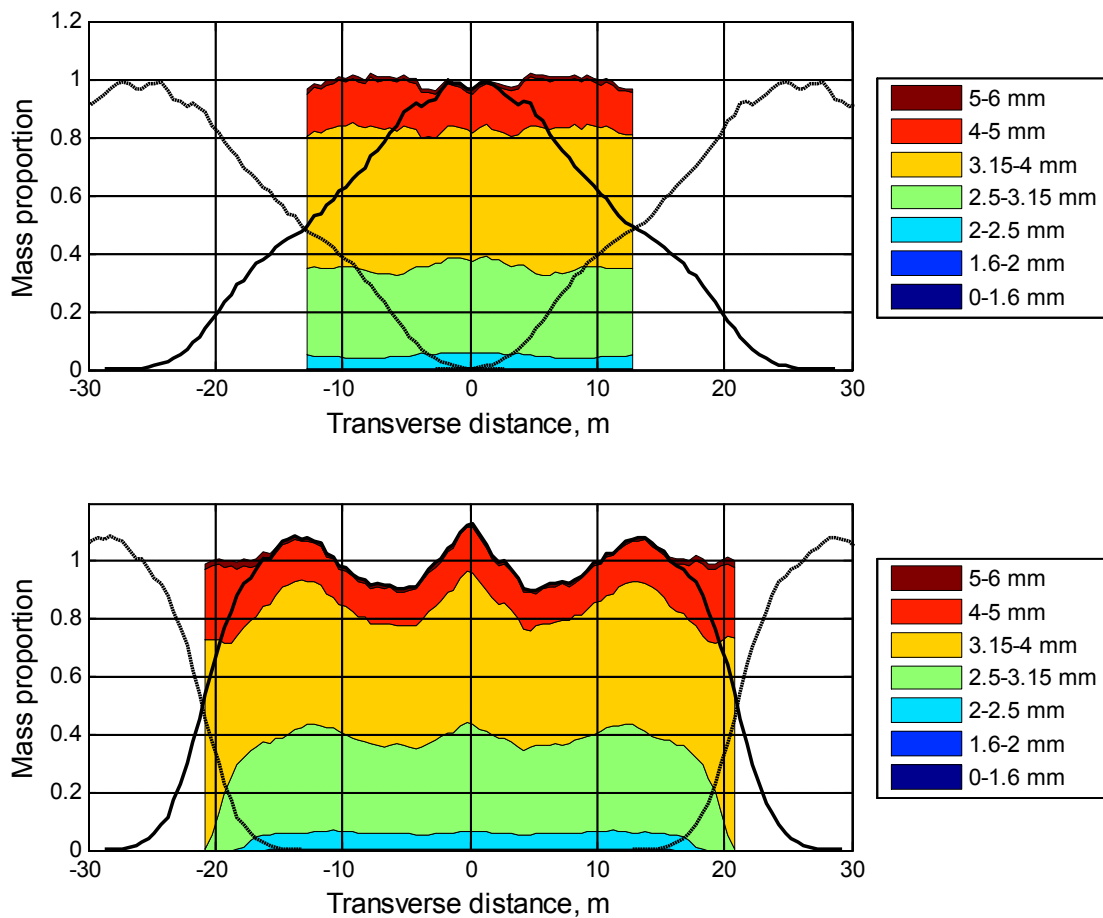
1 The differences observed here only result from the measurement procedure since no  
 2 additional perturbation (i.e. wind, ground topography, ground irregularity, guidance error...)  
 3 was taken into account for the “in field” measurements. Thus, the “in-field” CV defined in  
 4 this section should not be confused with the “field CV” defined by [Lawrence and Yule](#)  
 5 ([2007](#)).



6  
 7 Fig. 11 – Mean value and error bar (twice the standard deviation) of the CV with respect to  
 8 the application rate for the spreading situation SS2. Simulations are performed with collection  
 9 trays of 0.5×0.5 m for virtual “in-field” measurements (continuous line) and for virtual  
 10 “standard” measurements (dotted line).

11  
 12 **3.5 Influence of granule size and drag coefficient**

13  
 14 One particularity of the spread pattern simulations described in this article was that each  
 15 fertilizer granule was tracked during the whole virtual spreading process. Consequently, at the  
 16 end of the process, when all granules lied on the ground, the location and the diameter of each  
 17 granule were perfectly known. Thus, simulations were used to study how fertiliser particles  
 18 contribute to the transverse distribution in relation to their diameters. Figure 12 presents the  
 19 transverse distributions of the fertilizer sieve fractions for two spreading situations: SS2 and  
 20 SS5. For each situation, simulations have been performed with  $10^6$  fertiliser granules per disc.  
 21 The size of the virtual collection trays was 0.5×0.5 m. In the case of situation SS2, the  
 22 proportions of each diameter class are approximately kept constant on all the working width  
 23 (26 m) and correspond to the particle size analysis presented in Fig. 12. In this situation, the  
 24 transverse distribution has a triangular shape before overlapping and adjacent passes overlap  
 25 on a large part of the working width. In contrast, in the case of situation SS6, the proportions  
 26 of diameter classes are modified at the extremities of the working width with small diameter  
 27 vanishing. In this last situation, the swath spacing is 42 m, the transverse distribution has a  
 28 trapezoidal shape before overlapping and adjacent passes overlap only on a low part of the  
 29 working width. Thus, the overlapping area only concerns the external part of the spread  
 30 pattern and the landing points of biggest granules.

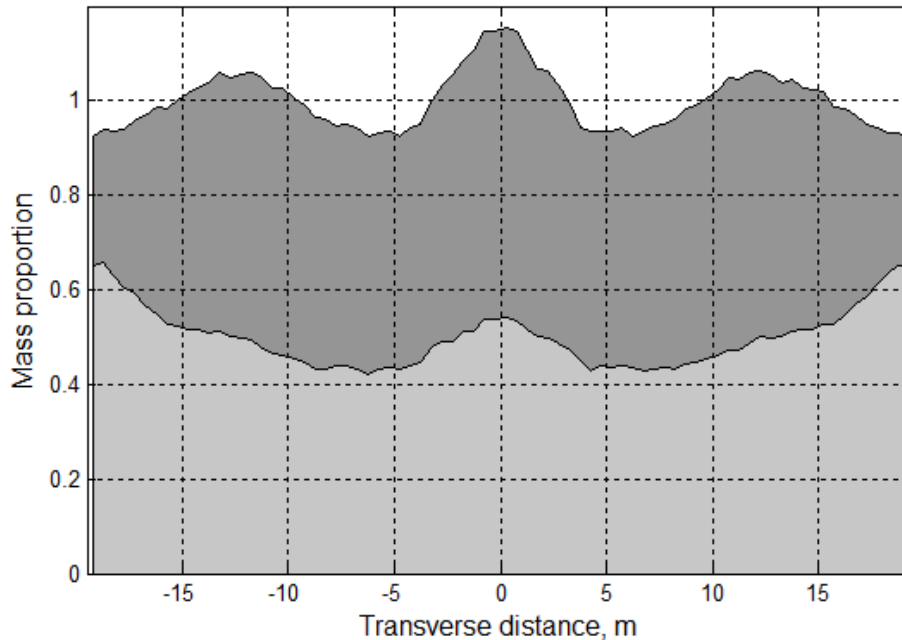


1  
2 Fig. 12 – Overlapped transverse distribution of fertiliser diameter classes on the working  
3 width, in the case of two spreading situations: SS2 (top) for a spacing width of 26 m and SS6  
4 (bottom) for a spacing width of 42 m. The transverse mass distributions are superposed for the  
5 central pass (continuous black line) and adjacent passes (dashed black line).  
6

7 In the case of situation SS6, the same rate (i.e. same mass per surface unit) is applied locally  
8 at 2.5 m and 21 m from the centerline of the virtual spreader, but the number of granules per  
9 surface unit is not the same. For the same application rate, the number of granules decrease  
10 when their sizes increase. Consequently, this affects the spatial variability of the fertiliser  
11 supply at very small scales. A further characterization of this effect is worth of studying but is  
12 out of scope for this article.

13 The study of spreading segregation is also of particular interest for blended fertilisers. The  
14 HCSM is an interesting tool to investigate how ballistic segregation affects the spatial  
15 distribution of each fertiliser components. To illustrate this aspect, a simulation was  
16 performed by considering two fertiliser components and one spreading situation. The first  
17 fertiliser component corresponded to ammonium nitrate whose characteristics had been  
18 described and used in the previous sections. The second fertiliser component corresponded to  
19 a fictive material, which only differ by the drag coefficient set at 0.60 (instead of 0.47 for the  
20 first component). This  $C_d$  value was the one used by [Grafton et al. \(2015\)](#). Considering that  
21 the two fertiliser components were in the same weight proportion, the simulation was carried  
22 out for a setting angle of  $-54^\circ$  and a swath spacing of 39 m. In these spreading conditions, Fig.  
23 13 shows the transverse distribution of the blended fertilisers and of each component. The CV  
24 computed for the blended fertilisers was 6.1 %. Nevertheless, the CV values were at least

1 twice when each fertiliser component was considered independently. Thus, the CV reached  
2 12.5% for the first component and 17.1% for the second one. This illustrates that the  
3 measurement of the CV for blended fertilisers (i.e. measured without differencing the  
4 components) does not systematically provide a good assessment of the spatial chemical  
5 variability.



6  
7 Fig 13. Overlapped transverse distribution of blended fertilisers that only differ in their  
8 respective drag coefficient: 0.47 (in light grey) and 0.60 in (in dark grey).  
9

10 The benefit of this approach is that results are not limited to comparison of the ballistic  
11 lengths of individual particles in contrast with works of [Antille et al. \(2015\)](#) or [Grafton et al.](#)  
12 [\(2015\)](#). The present approach considers the two-dimensional spread pattern so that the  
13 transverse distribution is computed taking into account the overlapping of adjacent passes.  
14

15 This section put the emphasis on the interest of HCSM to investigate the impact of fertiliser  
16 properties on the transverse distribution. The accurate study of a specific blended fertiliser  
17 would require to characterize the mechanical behavior of the mixture on the spinning disc to  
18 provide the horizontal and vertical outlet angle distributions and the angular mass flow  
19 distribution (as described in section 2.2). It would also required to characterize the properties  
20 of each fertiliser components in terms of specific density, diameter distribution and drag  
21 coefficient (as described in section 2.3). Using these input parameters, the HCSM would be an  
22 efficient and low cost strategy to study the behaviour of blended fertilisers and provide  
23 recommendations on swath spacing.  
24

#### 25 4. Conclusion

26  
27 To simulate fertiliser spread pattern depositions, a hybrid model was proposed. This approach  
28 combined the use of theoretical motion equations and experimental results. The experimental  
29 data were used to adjust few constant parameters and to provide the statistical distributions of  
30 other input parameters. This ensured the realistic nature of fertiliser mechanical behaviours  
31 and spread pattern simulations. The particularity of the hybrid model was the use of  
32 successive random selections to compute the spread pattern deposition of virtual particles  
33 whose size and motion parameters respected experimental statistical distributions. This Monte

1 Carlo process took into account the variability of input parameters and made possible the use  
2 of simulation replications to access to statistical characteristics of the output variables.  
3 Simulation results showed the Hybrid Centrifugal Spreading Model was worth of interest to  
4 study information that was difficult or impossible to access with actual experiments. In  
5 particular, results demonstrated the transverse CV not only depended on the spreader setting  
6 and the swath spacing but also increased when the application rate decreased. The CV value  
7 also increased when the collection tray surface decreased. A mathematical relationship had  
8 been derived from simulation results to describe these influences. The study also  
9 demonstrated the variability of CV measurements increased when the application rate or the  
10 collection tray length decreased. Differences observed in the CV value, when it was measured  
11 in field or following the standard specified in EN 13739-2, were highlighted.  
12 An insight into the distribution of the fertiliser particles related to their diameter or their drag  
13 coefficient showed the Hybrid Centrifugal Spreading Model will be a powerful tool to analyse  
14 further the impact of fertiliser ballistic properties on the spread pattern.  
15 More generally, the model and the associated Monte Carlo simulations open up the possibility  
16 of carrying out virtual and numerical experiments to avoid cumbersome experimental tasks  
17 for numerous research or development activities. For instance, this will be of particular  
18 interest in: studying the effects of perturbing factors such as wind; providing  
19 recommendations concerning the use of blended fertilisers for a selected swath spacing;  
20 comparing different test methods to assess the transverse distribution or the spread pattern  
21 (especially to design simplified tests); assessing the accuracy of test methods (especially in  
22 defining the optimal swath width); or defining the probability of obtaining a selected range of  
23 application rate for a selected spatial scale defined by agronomical criteria.  
24  
25

## 26 5. References

- 28 Antille, D.L., Gallar-Redondo, L., Godwin, R.J., 2013. Determining the particle size range of  
29 organomineral fertilisers based on the spreading characteristics of the material, ASABE  
30 Annual International Meeting, Kansas City, Missouri, July 21-July 24, 2013. American  
31 Society of Agricultural and Biological Engineers, p. 18.
- 32 Antille, D.L., Gallar, L., Miller, P., Godwin, R., 2015. An investigation into the fertilizer  
33 particle dynamics off-the-disc. *Applied Engineering in Agriculture* 31, 49-60.
- 34 Aphale, A., Bolander, N., Park, J., Shaw, L., Svec, J., Wassgren, C., 2003. Granular fertiliser  
35 particle dynamics on and off a spinner spreader. *Biosystems Engineering* 85, 319-329.
- 36 ASAE Standards S341.2, 1999. Procedure for measuring distribution uniformity and  
37 calibrating granular broadcast spreaders, ASAE, St. Joseph, Michigan, USA.
- 38 Australian Fertiliser Services Association, 2001. Accu-Spread - Code of practice for  
39 spreading, Glenthompson.
- 40 Bradley, M., Farnish, R., 2005. Segregation of Blended Fertiliser During Spreading: The  
41 Effect of Differences in Ballistic Properties, International Fertiliser Society. IFS, United  
42 Kingdom.
- 43 Casas, G., Mukherjee, D., Celigueta, M.A., Zohdi, T.I., Onate, E., 2015. A modular,  
44 partitioned, discrete element framework for industrial grain distribution systems with  
45 rotating machinery. *Computational Particle Mechanics*, 1-18.
- 46 Coetzee, C.J., Lombard, S.G., 2011. Discrete element method modelling of a centrifugal  
47 fertiliser spreader. *Biosystems Engineering* 109, 308-325.
- 48 Cool, S., Vangeyte, J., van Damme, J., Sonck, B., Pieters, J., van de Gucht, T., Mertens, K.,  
49 2015. Comparison of different spread pattern determination techniques, *Precision  
50 agriculture'15*. Wageningen Academic Publishers, p. 146.

- 1 Cunningham, F.M., 1963. Performance characteristics of bulk spreaders for granular fertilizer.  
2 Transactions of the ASAE 6, 108-0114.
- 3 Cunningham, F.M., Chao, E.Y., 1967. Design relationships for centrifugal fertilizer  
4 distributors. Transactions of the ASAE 10, 91-0095.
- 5 EN 13739-2, 2003. Agricultural machinery - Solid fertilizer broadcasters and full width  
6 distributors - Environmental protection - Part 2: Test methods., European Committee for  
7 Standardisation.
- 8 EN 13739-2, 2011. Agricultural machinery - Solid fertilizer broadcasters and full width  
9 distributors - Environmental protection - Part 2: Test methods, European Committee for  
10 Standardization, Bruxelles.
- 11 Fulton, J., Shearer, S., Chabra, G., Higgins, S., 2001. Performance assessment and model  
12 development of a variable-rate, spinner-disc fertilizer applicator. Transactions of the  
13 ASAE 44, 1071.
- 14 Gomez-Gil, J., de-Lozar-Escudero, A., Navas-Gracia, L., Ruiz-Ruiz, G., 2009. Analytical  
15 estimation of optimal operation variables of a centrifugal fertilizer distributor, using the  
16 gradient method on multiple seeds. *Agrociencia (Montecillo)* 43, 497-509.
- 17 Grafton, M., Yule, I., Robertson, B., Chok, S., Manning, M., 2015. Ballistic Modeling and  
18 Pattern Testing to Prevent Separation of New Zealand Fertilizer Products. *Applied  
19 Engineering in Agriculture* 31.
- 20 Griffis, C., Ritter, D., Matthews, E., 1983. Simulation of rotary spreader distribution patterns.  
21 Transactions of the ASAE 26, 33-37.
- 22 Grift, T., Hofstee, J., 2002. Testing an online spread pattern determination sensor on a  
23 broadcast fertilizer spreader. Transactions of the ASAE 45, 561-570.
- 24 Grift, T., Kweon, G., Hofstee, J., Piron, E., Villette, S., 2006. Dynamic Friction Coefficient  
25 Measurement of Granular Fertiliser Particles. *Biosystems Engineering* 95, 507-515.
- 26 Hoffmeister, G., Watkins, S., Silverberg, J., 1964. Fertilizer Consistency, Bulk Blending of  
27 Fertilizer Material: Effect of Size, Shape, and Density on Segregation. *Journal of  
28 Agricultural and Food Chemistry* 12, 64-69.
- 29 Hofstee, J.W., 1995. Handling and Spreading of Fertilizers: Part 5, The Spinning Disc Type  
30 Fertilizer Spreader. *Journal of Agricultural Engineering Research* 62, 143-162.
- 31 Horrell, R., Metherell, A., Ford, S., Doscher, C., 1999. Fertiliser evenness-losses and costs: a  
32 study on the economic benefits of uniform applications of fertiliser, New Zealand  
33 Grassland Association Conference, pp. 215-220.
- 34 Inns, F., Reece, A., 1962. The theory of the centrifugal distributor II: Motion on the disc, off-  
35 centre feed. *Journal of Agricultural Engineering Research* 7, 345-353.
- 36 ISO Standard 5690/1, 1985. Equipment for Distributing Fertilizers: Test Methods, part 1: Full  
37 width fertilizer distributors, International Organization for Standardization, Genève.
- 38 Jensen, D., Pesek, J., 1962. Inefficiency of fertilizer use resulting from nonuniform spatial  
39 distribution: II. Yield losses under selected distribution patterns. *Soil Science Society of  
40 America Journal* 26, 174-178.
- 41 Jones, J.R., Lawrence, H.G., Yule, I.J., 2008. A statistical comparison of international  
42 fertiliser spreader test methods - Confidence in bout width calculations. *Powder  
43 Technology* 184, 337-351.
- 44 Kweon, G., Grift, T.E., 2006. Feed Gate Adaptation of a Spinner Spreader for Uniformity  
45 Control. *Biosystems Engineering* 95, 19-34.
- 46 Lawrence, H., Yule, I., 2007. Estimation of the in-field variation in fertiliser application. *New  
47 Zealand Journal of Agricultural Research* 50, 25-32.
- 48 Mennel, R., Reece, A., 1963. The theory of the centrifugal distributor III: Particle trajectories.  
49 *Journal of Agricultural Engineering Research* 7, 78-84.

- 1 Miller, P.C., Audsley, E., Richards, I.R., 2009. Costs and effects of uneven spreading of  
2 nitrogen fertilisers, Conference of the International Fertiliser Society, Cambridge, UK,  
3 10th December 2009. International Fertiliser Society, pp. 1-24.
- 4 Miserque, O., Pirard, E., 2004. Segregation of the bulk blend fertilizers. *Chemometrics and*  
5 *intelligent laboratory systems* 74, 215-224.
- 6 New Zealand Fertiliser Quality Council, 2015. Spreadmark code of practice, Wellington New  
7 Zealand: Online publication. Retrieved from <http://www.fertqual.co.nz>.
- 8 Olieslagers, R., 1997. Fertilizer distribution modelling for centrifugal spreader design. PhD  
9 Thesis, nr. 341. aan de faculteit der landbouwwetenschappen, K. U. Leuven, Belgium.
- 10 Olieslagers, R., Ramon, H., De Baerdemaeker, J., 1996. Calculation of Fertilizer Distribution  
11 Patterns from a Spinning Disc Spreader by means of a Simulation Model. *Journal of*  
12 *Agricultural Engineering Research* 63, 137-152.
- 13 Parish, R., 1986. Comparison of spreader pattern evaluation methods. *Applied Engineering in*  
14 *Agriculture* 2, 89-93.
- 15 Parish, R., Chaney, P., Fuller, D., 1987. Comparison of laboratory methods of spreader  
16 pattern evaluation with agronomic response. *Applied Engineering in Agriculture* 3, 237-  
17 240.
- 18 Parish, R., de Visser, P., 1989. Technical Notes: Experimental Verification of the Effect of  
19 Collection Pan Width on Apparent Spreader Pattern. *Applied Engineering in*  
20 *Agriculture* 5, 163-164.
- 21 Patterson, D., Reece, A., 1962. The theory of the centrifugal distributor. I: Motion on the disc,  
22 near-centre feed. *Journal of Agricultural Engineering Research* 7, 232-240.
- 23 Pettersen, J., Svendsen, J., Øvland, S., 1991. A method of studying the influence of fertilizer  
24 particle size on the distribution from a twin-disc spreader. *Journal of agricultural*  
25 *engineering research* 50, 291-303.
- 26 Piron, E., Miclet, D., 2005. Centrifugal fertiliser spreaders: a new method for their evaluation  
27 and testing, Conference of the International Fertiliser Society, York, United Kingdom.  
28 The International Fertiliser Society, p. 22p.
- 29 Piron, E., Miclet, D., Villette, S., 2010. CEMIB: an innovative bench for spreader eco-design,  
30 AgEng 2010, International Conference on Agricultural Engineering, Clermont-Ferrand,  
31 France, p. 9 p.
- 32 Pitt, R., Farmer, G., Walker, L., 1982. Approximating equations for rotary distributor spread  
33 patterns. *Transactions of the ASAE* 25, 1544-1552.
- 34 Reumers, J., Tijsskens, E., Ramon, H., 2003. Experimental Characterisation of the Tangential  
35 and Cylindrical Fertiliser Distribution Pattern from a Spinning Disc: A Parameter  
36 Study. *Biosystems Engineering* 86, 327-337.
- 37 Richards, I.R., Hobson, R.D., 2013. Method of calculating effects of uneven spreading of  
38 fertiliser nitrogen. *International Fertiliser Society Proc. No. 734*.
- 39 Søgaard, H.T., Kierkegaard, P., 1994. Yield reduction resulting from uneven fertilizer  
40 distribution. *Transactions of the ASAE* 37, 1749-1752.
- 41 Tijsskens, B., van Liedekerke, P., Ramon, H., 2005. Modelling to aid assessment of fertiliser  
42 handling and spreading characteristics, Conference of the International Fertiliser  
43 Society, York, United Kingdom. The International Fertiliser Society.
- 44 Tissot, S., Miserque, O., Mostade, O., Huyghebaert, B., Destain, J., 2002. Uniformity of N-  
45 fertiliser spreading and risk of ground water contamination. *Irrigation and drainage* 51,  
46 17-24.
- 47 Tissot, S., Quenon, G., Miserque, O., 1999. Tolérance d'une culture de froment à l'égard de  
48 l'hétérogénéité d'épandage des engrais azotés. *Biotechnologie, Agronomie, Société et*  
49 *Environnement* 3, 247-252.

- 1 Van Liedekerke, P., Tijsskens, E., Dintwa, E., Anthonis, J., Ramon, H., 2006. A discrete  
2 element model for simulation of a spinning disc fertilizer spreader I. Single particle  
3 simulations. *Powder Technology* 170, 71-85.
- 4 Van Liedekerke, P., Tijsskens, E., Dintwa, E., Rioual, F., Vangeyte, J., Ramon, H., 2009. DEM  
5 simulations of the particle flow on a centrifugal fertilizer spreader. *Powder technology*  
6 190, 348-360.
- 7 Villette, S., Piron, E., Cointault, F., Chopinet, B., 2005. Centrifugal Spreading: an Analytical  
8 Model for the Motion of Fertiliser Particles on a Spinning Disc. *Biosystems*  
9 *Engineering* 92, 157-164.
- 10 Villette, S., Piron, E., Cointault, F., Chopinet, B., 2008. Centrifugal spreading of fertiliser:  
11 Deducing three-dimensional velocities from horizontal outlet angles using computer  
12 vision. *Biosystems Engineering* 99, 496-507.
- 13 Villette, S., Piron, E., Martin, R., Miclet, D., Jones, G., Paoli, J., Gée, C., 2013. Estimation of  
14 two-dimensional fertiliser mass flow distributions by recording granule impacts.  
15 *Biosystems Engineering* 115, 463-473.
- 16 Villette, S., Piron, E., Miclet, D., Martin, R., Jones, G., Paoli, J., Gée, C., 2012. How mass  
17 flow and rotational speed affect fertiliser centrifugal spreading: Potential interpretation  
18 in terms of the amount of fertiliser per vane. *Biosystems Engineering* 111, 133-138.
- 19 Virk, S.S., Mullenix, D.K., Sharda, A., Hall, J.B., Wood, C.W., Fasina, O.O., McDonald,  
20 T.P., Pate, G.L., Fulton, J.P., 2013. Case Study: Distribution uniformity of a blended  
21 fertilizer applied using a variable-rate spinner disc spreader. *Applied Engineering in*  
22 *Agriculture* 29, 627-636.
- 23 Walker, J., Grift, T., Hofstee, J., 1997. Determining effects of fertilizer particle shape on  
24 aerodynamic properties. *Transactions of the ASAE* 40, 21-27.
- 25 Yule, I., 2011. The effect of fertilizer particle size on spread distribution. NZ Centre for  
26 Precision Agriculture, Massey University, Palmerston North, New Zealand, 1-9.
- 27